SEMMELWEIS EGYETEM

DOKTORI ISKOLA

Ph.D. értekezések

3598.

BOD RÉKA BARBARA

Funkcionális Idegtudományok
című program

Programvezető: Dr. Sperlágh Beáta, egyetemi tanár

Témavezető: Dr. Wittner Lucia, tudományos tanácsadó

STRUCTURAL AND FUNCTIONAL ORGANIZATION OF HUMAN NEOCORTICAL MICROCIRCUITS

PhD thesis

Réka Barbara Bod, MD

Semmelweis University Doctoral College

Szentágothai János Neurosciences Division





Supervisor: Lucia Wittner, PhD, DSc

Official reviewers: Prof. József Csicsvári, PhD
Péter Ujma, PhD

Head of the Complex Examination Committee: Prof. Anita Kamondi, MD, DSc

Members of the Complex Examination Committee: Andrea Slézia, PhD
Orsolya Szalárdy, PhD

Budapest
2026

TABLE OF CONTENTS

TABLE OF CONTENTS 1
List of abbreviations 4
1. INTRODUCTION 5
1.1 Human cortical microcircuits 5
1.2 Human cortical dynamics: oscillations, population activity and their electrophysiological signatures 7
1.3 Human cortical dynamics across brain states and experimental contexts 11
1.4 From extracellular signals to single-neuron activity 13
1.5 Spike-field coupling and oscillatory coordination 15
1.6 Functional interactions and population organization 16
1.7 Histological correlates of human cortical microcircuits 17
1.8 Clinical context of human cortical recordings 18
2. OBJECTIVES 21
2.1 Structural and functional organization of excitatory microcircuits in the human epileptic neocortex 21
2.2 Functional organization of human cortical microcircuits in vivo and in vitro 21
3. METHODS 22
3.1 Study design 22
3.2 Human subjects and cortical tissue 23
3.2.1 Ethical approval 23
3.2.2 Patient cohorts 23
3.3 In vivo intracortical recordings 24
3.4 In vitro extracellular electrophysiology 25
3.4.1 Acute human cortical slice preparation 25
3.4.2 In vitro electrophysiological recordings 25
3.4.3 Pharmacological manipulation of glutamatergic neurotransmission 26
3.5 Spike sorting and postprocessing 26

3.5.1 SpikeWise: a graphical user interface for spike sorting postprocessing 27
3.6 Standard electrophysiological signal processing 28
3.6.1 Local field potential preprocessing 29
3.6.2 Current source density analysis 29
3.6.3 Single-unit waveform characterization and cell type classification 30
3.7 Oscillatory analyses 31
3.7.1 Spectral epoch detection 31
3.7.2 Spike-field coupling 31
3.8 Functional interactions and network analyses 32
3.8.1 Putative functional connectivity 32
3.8.2 Population coupling 32
3.8.3 Graph-theoretical analysis 32
3.8.4 Population dimensionality and activity-space structure 33
3.9 Histological analysis 34
3.10 Minimal analytical mesoscopic model 34
3.11 Statistical analysis 35
4. RESULTS 36
4.1 Structural and functional organization of excitatory microcircuits in the human epileptic neocortex 36
4.1.1 Spontaneous population activity in epileptic and non-epileptic neocortex 36
4.1.2 Glutamatergic contribution to spontaneous population activity 36
4.1.3 Single-neuron firing properties and cell-type composition 38
4.1.4 Neuronal recruitment during spontaneous population activity 40
4.1.5 Putative functional interaction readouts between neurons 41
4.1.6 Histological characterization of cortical organization 42
4.1.7 Summary of the findings for Objective 1. 43

4.2 Functional organization of human neocortical microcircuits in vivo and following experimental isolation..... 44

4.2.1 Isolation alters intrinsic excitability while preserving baseline firing..... 44

4.2.2 Cortical isolation enhances gamma-band spike-field synchronization 46

4.2.3 Enhanced gamma synchrony is accompanied by reduced population coupling and functional network integration..... 48

4.2.4 Histological preservation and dissociation of structure-function relationships. 51

4.2.5 A minimal mesoscopic model reproduces the dissociation between population coupling and gamma synchronization 54

4.2.6. Summary of the findings for Objective 2 55

5. DISCUSSION..... 57

5.1 Excitatory microcircuits and their reorganization in epilepsy..... 57

5.2 Local microcircuits versus large-scale network embedding..... 59

5.3 A unified view: local activity generation and distributed organization 60

5.4 Strengths and limitations 61

5.5 Translational and methodological implications..... 63

6. CONCLUSIONS 64

7. SUMMARY..... 65

8. REFERENCES 66

BIBLIOGRAPHY OF THE CANDIDATE'S PUBLICATIONS..... 80

ACKNOWLEDGEMENTS..... 81

LIST OF ABBREVIATIONS

aCSF - artificial cerebrospinal fluid

AMPA - α-amino-3-hydroxy-5-methyl-4isoxazolepropionic acid

APV – DL-2-amino-5-phosphonovaleric acid

B% – burstiness index quantifying the fraction of spikes occurring within bursts

B20 - burstiness index assessing the ratio of ISIs under 20 ms

CCG – crosscorrelogram

CSD – current source density

ECoG – electrocorticography

EEG - electroencephalography

FS – fast-spiking interneuron

IB-PC – intrinsically bursting principal cell

IN - interneuron

ISI CV – coefficient of variation of the inter-spike intervals

LFP – local field potential

LFPg – gadient local field potential (first spatial derivative of LFP)

NBQX - 2,3-dihydroxy-6-nitro-7-sulfamoyl-benzo(f)quinoxaline

NeuN – Neuronal nuclei (antibody)

NFS – non-fast-spiking interneuron

NMDA – N-methyl-D-aspartate

NREM – non-REM (rapid eye movement) sleep

PC1 – primary principal component

PLV – phase lock value

PV – parvalbumin

RS-PC – regularly spiking principal cell

SMI32 - antibody for non-phosphorylated neurofilament protein epitopes (168/200 kDa)

SPA – spontaneous population activity

1. INTRODUCTION

1.1 Human cortical microcircuits

The cerebral cortex provides the core neural substrate for perception, cognition, memory and voluntary behavior. Rather than operating through isolated clusters of neurons, cortical function emerges from the dynamic integration of densely interconnected microcircuits with the wider distributed networks of the brain. These microcircuits, however, represent the principal computational units of the cortex, where local recurrent processing and long-range cortico-cortical and subcortical communication similarly take place (1, 2).

Despite its remarkable expansion during primate evolution and the functional specialization of distinct cortical areas, the mammalian neocortex preserved a highly conserved six-layered organization (3). Canonical layers differ in their neuronal composition, projection targets, synaptic connectivity and intrinsic electrophysiological properties, this way enabling an established information flow across the well-described directional pathways (4). Feedforward inputs from lower-order cortical regions and the thalamus primarily terminate within the granular layer (layer IV) (5, 6), whereas feedback projections preferentially target superficial and deep cortical layers. Accordingly, supragranular neurons, in layers I-III, largely participate in corticocortical communication (7–9), while infragranular neurons (layers V-VI) provide the principal outputs to subcortical structures.

Dense recurrent connectivity is a signature of cortical microcircuits. Unlike purely feedforward systems, pyramidal neurons sustain extensive local excitatory connections due to their long-range projections, making thus possible the amplification of synaptic inputs, persistent activity, nonlinear computation and flexible transitions between versatile network states (10). Approximately three-quarters of cortical neurons are glutamatergic pyramidal cells, whereas the remaining population consists of highly diverse subpopulations of GABAergic interneurons. Although numerically less represented, interneurons exert a disproportionately large influence on cortical computation by regulating neuronal gain, spike timing and oscillatory synchronization, hence guarding over the balance between excitation and inhibition (11, 12).

Interneurons comprise of molecularly and functionally heterogeneous subclasses: parvalbumin-, somatostatin- and vasoactive intestinal peptid-expressing neurons

represent the major populations (13). These classes selectively target different subcellular compartments of pyramidal neurons: depending on whether the soma, dendrites and axon initial segment are benefiting of inhibitory inputs, interneurons exert complementary effects on synaptic integration and generation of action potentials. Regarded as a classical example of their class, fast-spiking parvalbumin-positive (PV) interneurons provide powerful perisomatic inhibition and are considered essential for the generation of gamma-band oscillations through recurrent excitatory-inhibitory interactions (14–16).

Recent advances in single-cell transcriptomics profoundly refined our understanding of cortical cell diversity. Large-scale molecular profiling revealed dozens of transcriptionally distinct neuronal populations within both excitatory and inhibitory lineages, many of which cannot be clearly identified using morphology or electrophysiology alone (17). Intriguingly, transcriptomic identity does not always foretell anatomical or physiological phenotype, signifying that neuronal classification is self-standingly multidimensional and requires the integration of molecular, morphological and functional information (18). Throughout this work, neuronal populations are therefore classified primarily according to extracellular electrophysiological characteristics and laminar position, complemented by histological analyses wherever data made this possible.

Cortical microcircuits should therefore be regarded not as static anatomical wiring diagrams but as dynamical systems, in which neuronal activity emerges from the interaction between intrinsic cellular properties, recurrent synaptic connectivity and continuously changing external inputs. Neuromodulatory systems together with long-range corticocortical and thalamocortical projections dynamically reshape local circuit activity, allowing the cortex to transition between different functional states, but also maintaining robust computation features (19, 20).

However, being aware that conventional organization of cortical microcircuits is conserved across mammals, the human neocortex exhibits several distinctive structural and physiological features. Human pyramidal neurons possess substantially larger dendritic arbors, increased synaptic complexity, prolonged membrane time constants and specialized dendritic integrative mechanisms compared with rodents, supporting extended temporal integration and enhanced computational ability (7, 8, 21–25). These

species-specific properties highlight that observations obtained in experimental animal models cannot always be directly extrapolated to the human cortex.

Throughout this thesis, layerwise organization of the human neocortex serves as a framework approach towards exploring neuronal firing, oscillatory synchronization, population interactions and cytoarchitectural organization. Instead of merely treating anatomy and physiology as separate levels of description, the subsequent chapters aim to give an outlook on how local cellular organization constrains the dynamical range blueprinted by cortical microcircuits, that are later modulated through various physiological and experimental conditions.

1.2 Human cortical dynamics: oscillations, population activity and their electrophysiological signatures

The anatomical organization of cortical microcircuits provides the foundation plan from which neuronal dynamics can emerge. Nonetheless, cortical function cannot be understood from static connectivity patterns alone, as neuronal computation depends on the continuous interaction between individual cellular activity, recurrent synaptic networks and large-scale brain states (26). Cortical activity is therefore a result of structured population dynamics rather than a framework for independent neuronal firing. These dynamics are expressed across multiple spatial and temporal orders of magnitude, ranging from millisecond-scale action potentials of individual neurons to large-scale oscillatory patterns of neuronal populations belonging to various brain regions (27).

A fundamental characteristic of cortical dynamics is the emergence of rhythmic activity (28). Neural oscillations reflect the coordinated activity of neuronal populations and arise through interactions between intrinsic cellular properties, synaptic connectivity and network architecture (29). Different frequency bands are associated with distinct physiological processes, although their functional roles are not strictly segregated (30). Slow oscillations coordinate large-scale transitions between active and inactive states during sleep (31), theta rhythms contribute to temporal organization of neuronal activity and memory-related processes (32), while beta and gamma oscillations are involved in sensory processing, attention, cortical communication and temporal coordination of neuronal ensembles (33).

Among cortical rhythms, gamma-frequency activity has received particular attention, mostly out of its close relationship with local circuit interactions. Gamma oscillations are

thought to emerge from reciprocal interactions between excitatory pyramidal neurons and fast-spiking inhibitory interneurons, particularly parvalbumin-expressing cells (14, 34–37). Through precisely timed inhibition, interneurons regulate the temporal window during which pyramidal neurons can discharge, allowing synchronization of neuronal populations and coordination of information processing (14, 33–35). Importantly, gamma oscillatory activity, as with other oscillations, is not generated by a single cellular element, but represents an emergent property of interconnected neuronal populations.

Oscillations are witnessed across multiple levels of cortical organization. Local field potentials (LFPs) reflect extracellular voltage fluctuations generated primarily by synchronized transmembrane currents associated with synaptic activity(38, 39). Because these signals integrate activity from populations of neurons within the vicinity of the recording electrode, they provide information about local network organization. In contrast, extracellular action potentials reflect the activity of individual neurons, allowing investigation of firing rates, spike timing and interactions between single neurons and surrounding population activity (40, 41). Combining these complementary signals enables investigation of how cellular activity contributes to emergent cortical dynamics.

Direct electrophysiological recordings from the human brain provide an exceptional opportunity to examine these processes in the species in which cognition and neurological disorders ultimately emerge. Although studies in rodents and non-human primates have established fundamental principles of cortical computation (42), substantial interspecies differences exist in neuronal morphology, intrinsic membrane properties, synaptic organization and network dynamics. Human principal cells and interneurons, with many species-specific subtypes, exhibit larger dendritic trees, prolonged membrane time constants and increased synaptic complexity compared with rodent neurons, suggesting that mechanisms regulating human cortical dynamics may not be fully captured by experimental models (43–47).

Human intracranial electrophysiology is primarily performed in patients undertaking neurosurgical procedures for pharmacoresistant epilepsy or tumor resection. In these clinical settings, invasive recordings may be obtained for functional mapping or localization of pathological tissue, providing access to neuronal activity with spatial and temporal resolutions otherwise unachievable through non-invasive approaches. This way, although clinical constraints limit experimental flexibility, recordings obtained from the

vicinity of non-pathological cortical regions provide a unique opportunity to investigate human cortical physiology directly (48, 49).

Different electrophysiological approaches offer a picture of different levels of cortical organization. Surface recordings, including electroencephalography (EEG) (50), electrocorticography (ECoG) (51) and intracranial electroencephalography, measure the summed electrical activity generated by large neuronal populations. Compared with EEG, subdural ECoG grids and strips provide superior spatial resolution, and have been exhaustively used to study cortical oscillations, functional connectivity and epileptic network organization. Still, these recordings integrate activity over relatively large cortical fields and therefore provide a limited access to local microcircuit mechanisms.

In contrast, intracortical microelectrodes and laminar probes enable recordings not only at the mesoscopic, but the cellular levels as well (52, 53). These electrodes simultaneously capture extracellular action potentials and local field potentials, allowing the investigation of the relationship between single-neuron firing and their surrounding network's activity. Laminar multichannel probes are particularly suited for studying cortical microcircuits, since they sample activity across all cortical layers (49, 54). This enables layer-specific analysis of neuronal firing, oscillatory activity and transmembrane current flow through current source density (CSD) analysis (55).

Extracellular recordings therefore provide complementary views on the various scales of cortical dynamics(56). High-frequency components of the signal contain action potentials generated by nearby neurons and can be separated into single-unit activity through spike sorting procedures(57–59). This data allow characterization of neuronal firing properties, spike timing and functional interactions between neurons(60). Lower-frequency components reflect synchronized synaptic activity within local populations and provide information about network-level dynamics through oscillatory analyses, spike-field coupling and population-level measures of synchrony.

An additional advantage of intracranial recordings is the possibility to investigate cortical activity across naturally occurring physiological states(61). Neuronal populations continuously reorganize their activity according to behavioral and internal states, including wakefulness and sleep. During wakefulness, cortical networks operate under continuous sensory input, cognitive demands and neuromodulatory influence(62, 63). During non-rapid eye movement (NREM) sleep, neuromodulatory conditions and

increased neuronal synchrony generate distinct oscillatory motifs that reshape cortical dynamics (31, 64). Long-term intracranial recordings hence provide a unique opportunity to examine how identical neuronal populations modify their activity while remaining nested within the intact human brain.

Despite these benefits, human intracranial recordings remain framed by constrained accessibility, small patient cohorts, clinically determined electrode placement and restricted experimental manipulation (65). Nevertheless, their ability to directly capture neuronal activity in the living human brain makes them indispensable for understanding how human cortical microcircuits generate coordinated activity(66).

In patients undergoing surgical treatment for drug-resistant epilepsy, the clinical evaluation provides an exceptional opportunity to study human cortical activity both in vivo and ex vivo. During presurgical monitoring, intracranial electrodes allow neuronal population activity to be examined within the intact brain, preserving physiological state, long-range connectivity, and interactions between distributed cortical and subcortical networks. However, since these recordings are primarily performed for clinical purposes, experimental manipulation is inevitably limited, and direct investigation of cellular and synaptic mechanisms is constrained. Following clinical evaluation, surgically resected cortical tissue can be rapidly transferred to the laboratory and prepared as acute cortical slices. In vitro recordings enable controlled investigation of local microcircuit properties, including pharmacological manipulation of synaptic transmission and analysis of individual neuronal and population activity. At the same time, the acute slice represents only a spatially restricted portion of cortex and lacks its original long-range connections, while tissue preparation may alter local physiology. Thus, in vivo and in vitro recordings provide complementary perspectives: the former preserves the intact network context, whereas the latter enables controlled investigation of locally preserved cortical circuits.

This work investigates how human neocortical dynamics are emerging across complementary experimental conditions. Chronic intracranial recordings provide access to neuronal activity within the intact brain during different physiological states, whereas acute recordings from surgically resected tissue allow the analysis of local circuit properties in isolation. Taken together, these approaches enable examination of how intrinsic microcircuit organization and large-scale network embedding contribute to the generation of human cortical dynamics.

1.3 Human cortical dynamics across brain states and experimental contexts

The activity of cortical microcircuits is constantly shaped by the global state of the brain. Although the connectomical foundations of the neocortex remain remarkably stable over smaller timescales, the same neuronal populations make swift transitions between distinct dynamical functions depending on arousal, behavioral context and states. These state-dependent changes influence neuronal firing, oscillatory synchronization, neuronal correlations, and the rise of population activity, thereby determining how information is represented and processed by cortical networks(67).

Wakefulness is characterized by highly dynamic cortical activity, shaped by continuous sensory input, cognitive demands, and widespread neuromodulatory influences (68). At the population level, the awake cortex often exhibits irregular and relatively asynchronous activity, that goes along with weak pairwise correlations and a broad variety of accessible network configurations (62). Specifically, this apparent randomness does not represent unstructured noise, the more plausible explanation is the high-dimensional dynamical neuronal coding state in which microcircuits constantly explore diverse activity patterns. Such dynamics allow cortical neuronal populations to remain responsive to changing external inputs, while simultaneously supporting internally generated patterns (69)

During non-rapid eye movement (NREM) sleep, cortical dynamics undergo a profound reorganization (70). Reduced neuromodulatory drive promotes alternating periods of population depolarization and hyperpolarization, commonly described as ‘Up‘and ‘Down*’* states, which generate prominent slow oscillations and widespread neuronal synchronization (71, 72). Compared with wakefulness, slow wave-sleep-associated activity is characterized by increased temporal coordination among neuronal populations and a more reduced repertoire of network interactions. Recent studies suggest that sleep represents a distinct dynamical establishment, in which enhanced synchrony exists along with altered population recruitment and reduced flexibility compared with the awake state (73, 74). The differences between wakefulness and sleep demonstrate that cortical dynamics cannot be solely investigated on the anatomical basis of local circuits. In its place, ongoing activity can be considered as an emergence from the interface between intrinsic microcircuit mechanisms and continuous modulation by large-scale networks, including corticocortical, thalamocortical, and neuromodulatory systems (75). Determining the relative contribution of local versus long-range or generalized

mechanisms remains a major challenge in human neuroscience, as these components are normally inseparable in the intact brain.

Acute cortical slice preparations provide a complementary experimental approach by preserving local recurrent connectivity while removing long-range inputs and behavioral influences. Consequently, spontaneous activity observed in isolated tissue primarily reflects the intrinsic properties of the local microcircuit, including recurrent synaptic interactions, intrinsic membrane properties, and local network organization (76). Comparison between intact and isolated preparations therefore offer a unique opportunity to determine which features of cortical dynamics are generated locally and which depend on integration within strewn brain networks.

Human cortical slice preparations are particularly valuable in this context because they preserve species-specific cellular properties that are not fully covered in experimental animals (4, 77, 78). Previous studies have demonstrated that human neocortical tissue remains spontaneously active after surgical resection, generating recurrent population events, oscillatory activity, and complex synaptic interactions (79, 80). However, because isolated tissue lacks continuous input from distant networks, the relationship between intrinsic human cortical dynamics and activity in the intact brain remains incompletely understood.

A direct comparison between these experimental conditions could therefore reveal how cortical dynamics emerge from the interaction between local circuitry and global network embedding. In one experimental framework employed in this thesis, neuronal activity was examined first in vivo during wakefulness and NREM sleep, and subsequently in vitro, following surgical isolation of tissue from the same cortical regions. This within-patient approach minimized inter-individual variability and enabled investigation of the same human microcircuit under different levels of network integration.

As an alternative to considering in vivo and in vitro recordings as interchangeable representations of cortical activity, this work attempted to interpret them as distinct functional states of the same anatomical substrate. The comparison granted this way allowed the investigation of a fundamental question in systems neuroscience: which properties of cortical dynamics arise intrinsically from local recurrent circuitry, and which require continuous interaction with the intact brain?

The analyses presented in this thesis address this question by examining neuronal firing properties, spike-field synchronization, functional connectivity, graph-theoretical organization, population dimensionality and cytoarchitectural features across the continuum from awake and sleeping human cortex to experimentally isolated cortical tissue.

1.4 From extracellular signals to single-neuron activity

The possibility of investigating cortical dynamics at a single-neuron level relies on extracellular electrophysiological recordings (Figure 1). Unlike intracellular techniques (81, 82), extracellular electrodes measure voltage fluctuations generated by transmembrane currents from multiple nearby neurons simultaneously (83, 84). As a result, the recorded signal contains information spanning multiple spatial scales: high-frequency components mainly reflect action potentials generated by individual neurons, whereas lower-frequency components constitute the local field potential (LFP), standing for the summed synaptic and membrane currents of local neuronal populations (38, 85). Modern microelectrodes therefore provide simultaneous access to neuronal output at the single-cell level together with the surrounding network activity, enabling investigation of cortical dynamics across multiple levels of organization (61, 86–88).

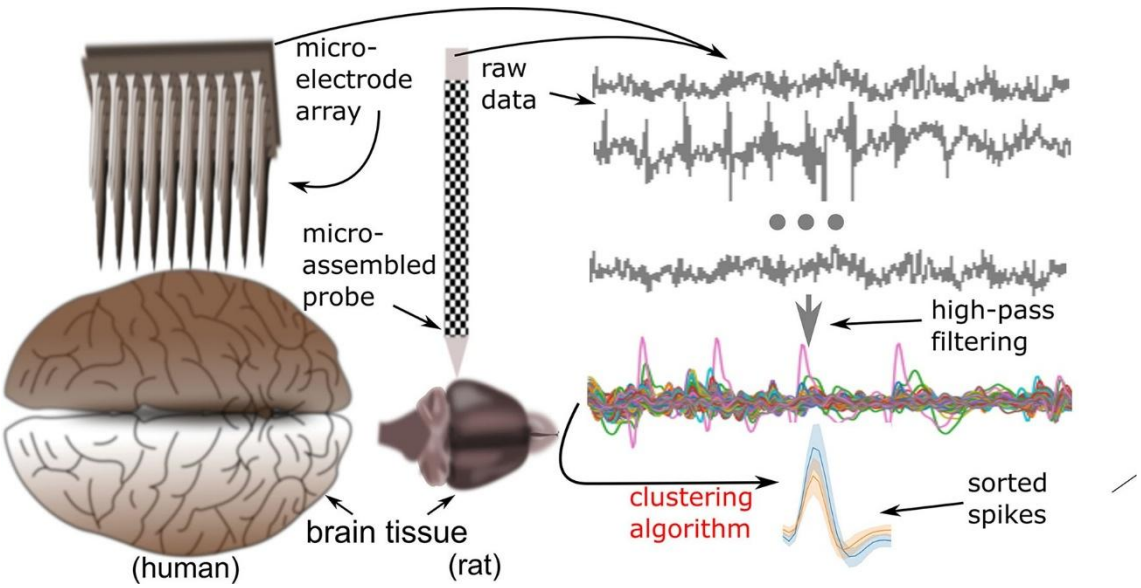


Figure 1. From brain to spike. *The acquisition, sorting, and analysis of single unit action potentials, coined as 'spikes' begin with recording neural signals from human or animal brain tissue. Microelectrode arrays and micro-assembled silicon probes are among the most used modalities for capturing these signals. The raw recordings are filtered to facilitate conventional spike-sorting procedures, enabling the identification of single-unit activities that are subsequently grouped into clusters based on waveform morphology. Image reused from,* ***Article I*** *(89), under CC-BY-4.0 license.*

Because each recording site detects activity from several neurons, extracellular recordings must be computationally decomposed into the spike trains of individual cells before any cellular-level interpretations take place. This process, known as spike sorting, consists of detecting extracellular action potentials, extracting informative waveform features, grouping spikes originating from the same neuron, and evaluating the quality of the resulting neuronal clusters (90). Over the past decade, spike sorting has evolved from relatively simple clustering approaches based on waveform amplitude and principal component analysis toward template-matching algorithms capable of resolving densely packed neuronal populations, along with gradual waveform drift compensation during long recordings (91, 92).

For this reason, reliable spike sorting set the ground for virtually every subsequent analysis performed on extracellular recordings. Inaccurate isolation of neuronal units directly influences estimates of firing rates, spike timing, neuronal correlations and temporal stability, thereby propagating errors into higher-order analyses of spike-field synchronization, functional connectivity, population coupling and graph-theoretical organization. Accordingly, robust quality assessment is a prerequisite for studying cortical microcircuits and interpreting interactions between neurons and neuronal populations. Although automated spike sorting algorithms have achieved remarkable performance, complete automation remains difficult, particularly in human recordings (93–96). Human cortical datasets frequently exhibit low signal-to-noise ratios, waveform drift during prolonged recordings, overlapping action potentials and substantial biological variability arising from the diversity of cortical cell types. Furthermore, unlike many experimental animal models, human recordings generally lack an independent ground truth against which sorting accuracy can be validated (97). For these reasons, automated clustering is typically complemented by manual or semi-automated curation based on multiple quality metrics, including waveform consistency, refractory-period violations, temporal stability, autocorrelograms and cluster similarity.

Recent years have witnessed rapid advances in both spike sorting algorithms and standardized evaluation frameworks: template-matching approaches have substantially improved the accuracy and scalability of extracellular data processing, while benchmarking initiatives including SpikeForest have enabled objective comparison of algorithmic performance across diverse recording conditions (98–100). At the same time,

increasing recording density and dataset complexity have shifted attention from automated clustering alone toward the broader problem of standardized post-processing, quality control and reproducible data analysis.

These developments motivated the systematic review of contemporary spike sorting methodologies and extracellular data analysis pipelines presented by our first article in the topic (89), which summarized the complete analytical workflow from signal acquisition and spike detection to quality assessment, visualization and downstream network analyses. Building upon this philosophy, filling up the gaps between contemporary algorithms and our data particularities, a graphical user interface was developed to facilitate transparent and standardized manual curation of spike sorting results. The software, presented in detail in Methods, integrates complementary quality metrics within a unified visualization environment, enabling efficient evaluation of cluster quality and improving the reproducibility and consistency of extracellular analyses across different datasets.

Throughout this thesis, all extracellular recordings underwent template-matching based spike sorting, quality-control and curation, which were complemented with the graphical user interface-based manual curation for the second topic of this thesis, all before downstream analyses were performed. This standardized workflow provides a solid foundation for the subsequent investigation of, thoroughly presented in the following chapters.

1.5 Spike-field coupling and oscillatory coordination

Neuronal firing does not happen in a vacuum, instead it is often temporally coordinated with ongoing oscillatory activity(101, 102). These oscillations, reflected in the LFP, arise from synchronized synaptic currents within neuronal populations, and grant a temporal framework that modulates neuronal excitability. To put it simply, oscillatory activity does not only influence individual firing rates, but it provides a temporal context, in this manner coordinating communication along local/distributed cortical networks (29, 103).

Spike-field coupling quantifies the relationship between the timing of action potentials and the phase of ongoing oscillations. Since oscillations reflect the collective activity of neuronal populations, but spikes represent the output of individual neurons, spike-field coupling provides a direct link between cellular and network dynamics. The strength and timing of this relationship can vary according to oscillatory frequency, cortical layer,

neuronal identity and behavioral state, providing insight into how individual neurons participate in coordinated population activity (104, 105). One of the most widely used measures of spike-field synchronization is the phase-locking value (PLV), which quantifies the consistency with which spikes occur at a particular phase of an oscillation. The preferred firing phase is described by the angle of the mean resultant vector, while the vector length reflects the concentration of spike phases and therefore the strength of phase locking, thus having two features of circular statistics accounting for both the magnitude and temporal description of spike-field interactions.

Interpretation of spike-field coupling requires careful consideration of the underlying physiological mechanisms. Strong phase locking does not necessarily imply that oscillations directly drive neuronal firing, but one must consider that coupling may arise because neurons receive common rhythmic synaptic input, participate in local excitatory-inhibitory circuits that generate oscillations, or are jointly influenced by broader network activity (106, 107). As a result, spike-field coupling is most informative when interpreted together with complementary measures describing neuronal interactions and network organization, therefore it follows to be assessed across multiple frequency bands, with particular emphasis on state-dependent changes between wakefulness, NREM sleep and isolated cortical tissue. These analyses address whether experimentally isolated human cortical microcircuits preserve rhythmic coordination observed in vivo, and how alterations in oscillatory synchronization relate to changes in local network organization.

1.6 Functional interactions and population organization

In the previous chapter, spike-field coupling was employed to describe the relationship between individual neurons and ongoing network oscillations. Moving forward, it is also useful to explore which interactions among neurons can be investigated directly through their temporal firing relationships. Crosscorrelograms (CCGs) quantify the relative timing of spikes between pairs of neurons and can reveal precise temporal interactions occurring over millisecond-timescales. Short-latency peaks or troughs may indicate putative excitatory or inhibitory synaptic interactions, although such interpretations remain indirect because common synaptic input, oscillatory synchronization and recording artefacts may produce similar correlation structures (60), this way extracellular recordings provide estimates of putative functional connectivity, but not direct evidence of monosynaptic connections.

Beyond pairwise interactions, cortical microcircuits exhibit coordinated activity at the population level. Population coupling quantifies the degree to which the firing of an individual neuron covaries with the activity of the surrounding neuronal ensemble (67, 108). Highly coupled neurons discharge in close coordination with local population activity, whereas weakly coupled neurons exhibit relatively independent firing patterns. Population coupling therefore provides insight into the functional role of individual neurons within local circuit dynamics and has emerged as an important descriptor of cortical network organization.

Network interactions can be further represented using graph-theoretical approaches, in which neurons are considered as nodes connected by edges representing functional relationships derived from spike timing, oscillatory synchronization or other measures of neuronal interaction. Graph-theoretical metrics, including node degree, strength, clustering coefficient, and hubness provide quantitative descriptions of network organizations that extend beyond individual neuronal pairs. Because different definitions of functional connectivity emphasize different physiological processes, comparison of graph structures derived from spike timing, phase synchronization and population coupling offers additional perspectives on cortical microcircuit organization (109, 110).

Recent work has also emphasized that neuronal populations occupy low-dimensional activity manifolds whose organization changes according to experimental conditions. This approach can offer an alternative of exploring all theoretically possible firing patterns: cortical populations should be treated as circuits operating within constrained dynamical subspaces that reflect the balance between recurrent local interactions and external network input (111, 112). Taken together, these analytical descriptors propose additional characterization of the human cortical microcircuits across wakefulness, sleep and experimental isolation. Putative connectivity, population coupling, graph-theoretical organization and population dimensionality are further examined together to determine how local recurrent circuitry and large-scale network embedding mutually shape neuronal interactions and emergent cortical dynamics.

1.7 Histological correlates of human cortical microcircuits

Electrophysiological recordings give an insight into the functional activity of cortical circuits; however, they do not directly reveal the cellular architecture from which these dynamics emerge. Histological analyses, on the other hand, provide an essential

anatomical framework for interpreting neuronal activity by quantifying the structural organization of the investigated cortical regions. Putting all together, integrating electrophysiological and histological measurements enables structure-function relationships to be examined across multiple spatial scales, linking cellular composition with emergent network dynamics (113). The human neocortex exhibits pronounced laminar variation in neuronal density, cell morphology and inhibitory interneuron distribution, all of which influence local connectivity and the balance between excitation and inhibition. Immunohistochemical markers provide complementary information about these anatomical features. Neuronal nuclei antibody (NeuN) labels the somata of mature neurons and enables quantitative evaluation of neuronal density along with layerwise architecture assessment. Parvalbumin (PV) marks a relatively homogeneous class of fast-spiking interneurons that provide perisomatic inhibition and drive gamma-oscillation synchrony, and their tight molecular-functional correspondence makes them particularly suitable for histology (114, 115). SMI32, an antibody recognizing non-phosphorylated neurofilament H, selectively labels subclasses of pyramidal neurons, particularly large cortico-cortical and corticofugal projection neurons, and has been extensively used to characterize laminar organization, cortical architecture and pathological alterations in human neocortex (116, 117). These immunohistochemistry markers thus provide a multidimensional description of cortical architecture, involving neuronal abundance, inhibitory circuitry and organization of projection neurons. Such anatomical information facilitates interpretation of electrophysiological findings and can reflect on the latent links between local cellular composition and electrophysiological signatures in neuronal firing, oscillatory synchronization and functional network organization.

As such, a highlight of this work was to relate local anatomical organization to cortical dynamics across discrete physiological and experimental conditions. Histological measurements are accordingly integrated with electrophysiological analyses to examine how neuronal density, inhibitory interneuron distribution, coverage and pyramidal neuron organization relate to neuronal firing properties, spike-field synchronization, functional connectivity and population-level network organization.

1.8 Clinical context of human cortical recordings

Direct investigation of human cortical physiology is essentially restricted to patients undergoing neurosurgical treatment, where invasive electrophysiological recordings or

surgical tissue resection are performed as part of routine clinical care. As a result, much of our current understanding of human cortical microcircuits derives from studies involving patients with pharmacoresistant epilepsy or intracranial tumors, including diffuse gliomas and brain metastases (118, 119). Although these clinical conditions impose unavoidable limitations, they provide a rare opportunity to investigate human cortical function with spatial and temporal resolution that cannot be achieved using non-invasive methods. In patients with pharmacoresistant epilepsy, intracranial recordings are performed to localize the seizure onset zone and guide surgical treatment (55, 120, 121). These recordings enable investigation of neuronal activity during natural wakefulness and sleep while anatomical and functional organization of the cortex is theoretically intact. In addition to all these, whenever possible, research analyses focus on cortical regions outside the epileptogenic zone to minimize the influence of seizure-related pathology on physiological measurements.

Acute cortical slices are commonly prepared from the tissue resected during surgery for epilepsy as well as for intrinsic brain tumors or metastatic lesions (122, 123). In tumor surgery, tissue suitable for research is typically obtained from cortical regions that must be removed to achieve the planned surgical approach or lesion resection rather than from the tumor itself. Careful neuropathological assessment therefore permits investigation of cortical tissue that is considered structurally preserved despite its clinical origin. Nevertheless, potential effects of the underlying disease, peritumoral changes, and patient-specific factors remain important considerations when interpreting experimental findings (124). Although recordings obtained during neurosurgical procedures cannot be regarded as originating from completely healthy individuals, numerous studies have demonstrated that non-pathological cortical tissue collected outside the primary lesion retains the characteristic anatomical, electrophysiological and transcriptomic properties of human neocortex (125). Such preparations have therefore become the principal experimental platform for studying human cortical physiology and have yielded fundamental insights into neuronal diversity, intrinsic membrane properties, synaptic connectivity and cortical dynamics (126, 127). The studies presented in this thesis build upon these complementary clinical paradigms. Chronic intracranial recordings obtained from epilepsy patients are combined with acute electrophysiological and histological investigations of resected cortical tissue from patients undergoing surgery for epilepsy or

intracranial tumors. This way, the approaches, methods and analytical background illustrated in the previous chapters provide a rare opportunity to examine human cortical microcircuits across multiple experimental conditions while maintaining relevance to human neurobiology.

2. OBJECTIVES

Human cortical microcircuits generate neuronal activity through the interaction of recurrent local circuits integrated in large-scale brain networks. Although their cellular organization has been extensively studied, considerably less is known about how human cortical microcircuits generate coordinated activity under physiological conditions, how these dynamics depend on distant network interactions, and finally how they are altered in epilepsy. Accordingly, this thesis addresses two definite research objectives:

2.1 Structural and functional organization of excitatory microcircuits in the human epileptic neocortex

The 1st objective was to determine how pharmacoresistant epilepsy affects excitatory neurotransmission and local cortical microcircuit organization by combining extracellular electrophysiology with quantitative histological analyses. peculiarly, the study aimed to:

- explore the **contribution of glutamatergic neurotransmission** to spontaneous cortical activity in epileptic and non-epileptic human neocortex
- compare the **electrophysiological properties** and **putative connectivity profiles** of neuronal populations under pharmacological manipulation
- determine whether epilepsy is associated with **alterations** in **neuronal density** and the organization of excitatory cortical circuitry, on the grounds of histology

2.2 Functional organization of human cortical microcircuits in vivo and in vitro

The 2nd objective investigated the distinct contributions of intrinsic local circuitry and large-scale brain networks on human cortical dynamics. Aims included to:

- characterize **neuronal firing properties** across experimental conditions
- measure **oscillatory synchronization** and **spike-field coupling**
- compare **functional connectivity**, **population coupli**ng and network organization
- evaluate changes in **population dimensionality** and **signal complexity**
- identify laminar **gamma-band generators** using current source density analysis
- relate **electrophysiological** findings to layer-specific **histological** characteristics

Both objectives provide a multiscale portrayal of human cortical microcircuits through integration of cellular electrophysiology, network dynamics and quantitative histological analysis. Thus, the overarching aim was to tell apart dynamics generated by local cortical circuitry from those emerging through interactions with brain networks, while identifying how these mechanisms, especially their excitatory components, are modified in epilepsy.

3. METHODS

3.1 Study design

The work presented herein combines complementary in vivo, in vitro, histological and computational approaches to study the organization and dynamics of human cortical microcircuits in various physiological and experimental conditions. Instead of interpreting them as a set of independent studies, the datasets forming the grounds of the thesis were designed to address different levels of the same biological question: how intrinsic microcircuit properties interact with network embedding and rely on local structural signatures to shape neuronal activity in the human neocortex.

The first experimental study (128)**Article II**) examined how pharmacoresistant epilepsy changes excitatory neurotransmission and local cortical microcircuit configuration. Extracellular recordings from human cortical slices were investigated under pharmacological manipulation of glutamatergic neurotransmission, further supplemented by quantitative histological analyses to compare epileptic and non-epileptic neocortex. We placed particular emphasis on neuronal firing properties, putative functional connectivity, spontaneous population activity, and layer-specific neuronal organization.

The second study (**Preprint**) investigated the contributions of intrinsic local circuitry and large-scale brain networks to human cortical dynamics. Laminar multichannel recordings were acquisitioned in vivo during wakefulness and NREM sleep and compared afterwards with recordings from acute cortical slices prepared from the same cortical regions following surgical excision. This within-patient experimental design also enabled direct comparison of neuronal firing, further analyzed in the context of oscillatory synchronization, spike-field coupling, functional connectivity, population coupling, network topology, population dimensionality, current source density, and histological organization across experimental conditions.

All extracellular recordings underwent a unified analytical pipeline comprising automated spike sorting, standardized quality assessment and expert-guided manual curation before downstream analyses were performed. The methodological principles underlying this workflow were established in our previous review of extracellular electrophysiology and spike sorting ((89) **Article I**), while the graphical user interface developed to facilitate standardized post-processing is described in Section 3.5.

Electrophysiological analyses were enriched by quantitative histological assessment of the recorded cortical tissue using immunohistochemical markers of neuronal density and cellular identity. Integration of anatomical and physiological measurements enabled investigation of structure-function relationships across cortical layers and experimental conditions.

Because this thesis is built on published work and a submitted manuscript, and is strictly constrained to a 60-page format, methodological procedures described in detail elsewhere are presented here only to the extent necessary for understanding the experimental design and analyses. Comprehensive descriptions of experimental protocols, data acquisition, signal processing, pharmacological procedures, histological methods, and statistical analyses are available in **Article II**, the **Preprint**, and previously published papers from our laboratory(113, 129, 130), to which the reader is referred where appropriate. The postprocessing framework is made accessible through a GitHub repository, further codes to replicate findings are available upon request.

3.2 Human subjects and cortical tissue

3.2.1 Ethical approval

All experimental procedures were carried out in accordance with the Declaration of Helsinki and were approved by the appropriate institutional and governmental ethics committees, under (20680-2/2011/EKU, ETT TUKEB 206804/2012/EKU, IV/8358-3/2021/EKU, comprising patient cohorts recruited for independent research projects approved under separate ethical protocols). Written informed consent was obtained from all participants prior to inclusion in the study.

3.2.2 Patient cohorts

Human cortical recordings and tissue samples were obtained from patients undergoing neurosurgical interventions at the National Institute of Clinical Neurosciences, now Clinic for Neurosurgery and Neurointervention, Semmelweis University, Budapest. Depending on the objectives of the individual studies, patients underwent surgery either for pharmacoresistant focal epilepsy or for intracranial tumors. Relevant patient informations are included in Table 1 (**Article II.**) and Table 2 + Figure 7A (**Preprint**).

*Table 1 Clinical characteristics of patients included in **Article II.***

Patient code	Sex	Age (yrs)	Epilepsy onset (yrs)	Diagnosis	Epilepsy	Cortical region
E2	F	21	2	Focal cortical dysplasia with glioneural heterotopia	Yes	Frontal
E4	M	24	4	Ganglioglioma (WHO grade I)	Yes	Temporal

E5	F	18	5	Focal cortical dysplasia IIb	Yes	Temporal
E6	M	51	50	Hippocampal sclerosis	Yes	Temporal
E12	M	40	35	Hippocampal sclerosis	Yes	Temporal
E13	F	53	40	Hippocampal sclerosis	Yes	Temporal
E15	M	35	34	Focal cortical dysplasia with hippocampal sclerosis	Yes	Temporal
T6	M	31	—	Cavernoma with acute intracerebral hematoma	No	Frontal
T7	F	58	—	Glioblastoma (WHO grade IV)	No	Temporal
T8	F	78	—	Glioblastoma/astrocytoma (WHO grade IV)	No	Temporal
T17	F	74	—	Glioblastoma with oligodendroglioma components	No	Frontal
T20	F	59	—	Breast carcinoma metastasis	No	Frontal
T21	F	69	—	Kidney carcinoma metastasis	No	Parietal

*Table 2 Clinical characteristics of patients included in the **Preprint**.*

Patient code	**Sex**	**Age (yrs)**	**Epilepsy onset (yrs)**	**Diagnosis**	**Epilepsy**	**Cortical region**
Pt1	M	13	5	Focal cortical dysplasia	Yes	Right postcentral gyrus (parietal)
Pt2	F	31	18	Focal cortical dysplasia IIb with balloon cells	Yes	Right postcentral sulcus (parietal)
Pt3	M	48	39	Focal cortical dysplasia IIb with tuberous sclerosis	Yes	Left frontocentral
Pt4	F	46	35	Focal cortical dysplasia Ib/IIa	Yes	Left superior frontal gyrus
Pt5	F	18	15	Focal cortical dysplasia IIb with balloon cells	Yes	Right frontal
Pt6	M	30	27	Focal cortical dysplasia IIb with balloon cells	Yes	Right parietal
Pt7	M	32	23	Focal cortical dysplasia IIb with balloon cells	Yes	Right parietal
Pt8	M	42	—	Tuberous sclerosis	Yes	Right parietal

Intracranial laminar recordings performed in vivo were obtained from patients with pharmacoresistant epilepsy undergoing invasive presurgical monitoring for localization of the seizure onset zone. Acute cortical slice experiments included surgically resected neocortical tissue, received from subsequent operations for pharmacoresistant epilepsy, as well as for intracranial tumors.

3.3 In vivo intracortical recordings

In vivo extracellular recordings analyzed in the **Preprint** were obtained during invasive presurgical monitoring of patients with pharmacoresistant focal epilepsy. In addition to clinically indicated subdural electrocorticography (ECoG) electrodes, a 24-channel linear laminar microelectrode (55) was implanted perpendicular to the cortical surface beneath the clinical grid, enabling simultaneous recordings across the entire cortical thickness. The microelectrode had a shaft diameter of 350 µm, 40 µm recording contacts spaced at 150 µm intervals, and was insulated with polyimide-epoxy, located within a medical grade stainless steel needle, provided with a silicone cap on the top, thus enabling the electrode to move together with the surrounding brain tissue. Recordings were acquired continuously for up to 5-7 days during intracranial monitoring. Signals were amplified, bandpass filtered (0.01 Hz-10 kHz), and digitized at 20 kHz. Each recording channel measured the local field potential gradient (LFPg) relative to the adjacent contact, thereby

reducing volume-conducted activity and emphasizing translaminar potential differences. Electrode locations were verified with photographic documentation, and in selected cases, additional histological reconstruction following surgical resection. For analysis, only physiologically stable interictal recordings were included: approximately 30-minute artifact-free segments of resting wakefulness and NREM sleep were selected for each patient, without any seizures occurring within one hour before or after the analyzed recording periods. The analyzed recordings originated from cortical regions subsequently resected during therapeutic surgery, enabling direct comparison with in vitro recordings derived from the same cortical areas.

3.4 In vitro extracellular electrophysiology

3.4.1 Acute human cortical slice preparation

Acute neocortical slice preparations were derived from surgically resected tissue, handled immediately after neurosurgical procedures (similarly for **Article II** and **Preprint**). The tissue was transferred from the operating room to the laboratory in an ice-cold, oxygenated sucrose-based artificial cerebrospinal fluid (aCSF) containing (in mM): 248 sucrose, 26 $NaHCO_3$, 1 KCl, 1 $CaCl_2$, 10 $MgCl_2$, 10 glucose and 1 phenol red, continuously equilibrated with 95% O_2 and 5% CO_2. Coronal neocortical slices (500 µm) were prepared using a vibratome (Leica VT1000S) and subsequently maintained in an interface-type recording chamber at 32–35 °C. Slices were continuously perfused with standard physiological aCSF containing (in mM): 124 NaCl, 26 $NaHCO_3$, 3.5 KCl, 1 $MgCl_2$, 1 $CaCl_2$ and 10 glucose, equilibrated with 95% O_2 and 5% CO_2. Electrophysiological recordings were launched following recovery of the slices. Detailed slice preparation procedures have been described previously in (131).

3.4.2 In vitro electrophysiological recordings

Extracellular recordings from acute cortical slices were gained using the 24-channel linear laminar microelectrode, identical in recording geometry to that employed for the in vivo experiments, except that the in vitro probe lacked the silicone stabilization cap and possessed a longer, hockey-stick fashion shaft to facilitate positioning within cortical slices (55, 131). The electrode was positioned perpendicular to the pial surface, and recordings were obtained from multiple locations across each slice. Signals were amplified (0.01-10 000 Hz), digitized to 20 kHz using a 16-bit acquisition system, and stored for offline analysis. Depending on cortical thickness, recording contacts typically

sampled supragranular layer from contacts 1-8, granular layer between 9-13 and infragranular layer from 14-24, slices differing from average thickness were extrapolated according to electrode span, but laminar assignment was verified individually for each specimen. The **Preprint** analyzed spontaneous neuronal activity under baseline recording conditions only, thus no pharmacological agents were applied in these experiments.

3.4.3 Pharmacological manipulation of glutamatergic neurotransmission

Pharmacological experiments were performed exclusively in **Article II** to investigate the contribution of ionotropic glutamate receptors to spontaneous cortical activity. Following an initial control recording period (typically 5–10 min), NMDA receptors were blocked by bath application of DL-2-amino-5-phosphonovaleric acid (APV, 50 μM). Subsequently, AMPA/kainate receptors were inhibited by adding 2,3-dihydroxy-6-nitro-7-sulfamoyl-benzo[f]quinoxaline (NBQX, 5 μM) while maintaining APV in the perfusion cocktail. Finally, slices underwent a washout period under standard recording solution (Figure **3**B). Continuous extracellular recordings were acquired throughout the control, pharmacological and washout phases, allowing direct within-slice comparison of neuronal firing and population activity under different glutamatergic conditions. APV and NBQX were obtained from Tocris Bioscience (Bristol, UK), but complete experimental details are provided in **Article II**.

3.5 Spike sorting and postprocessing

Reliable identification of single neurons from extracellular recordings is a prerequisite for all successive analyses of neuronal firing, oscillatory synchronization and network interactions. Since each extracellular recording channel can potentially capture action potentials from several nearby neurons, broadband signals are routinely subjected to a standardized spike-sorting workflow comprising signal preprocessing, automated spike detection and clustering, followed by systematic quality assessment and manual curation. The general analytical framework employed throughout the works of thesis follows the ideas and best practices summarized in our methodological review of extracellular electrophysiology and spike sorting (**Article I,** (89)), which discusses current spike-sorting algorithms, validation strategies and quality control procedures for human recordings. Based on these considerations, only well-isolated units satisfying predefined quality criteria were included in downstream analyses.

Although the same general principles were applied throughout the thesis, the spike-sorting strategy differed according to recording conditions. **Article II** analyzed extracellular recordings obtained from acute cortical slices, where recordings were characterized by relatively high signal-to-noise ratio, limited electrode drift and stable waveform morphology over shorter recording time intervals. Automated spike sorting was therefore performed using the SpikeInterface framework (132)with the Tridesclous algorithm (https://github.com/tridesclous/trisdesclous), followed by manual inspection and curation using Phy (https://github.com/cortex-lab/phy).

On the other hand, the **Preprint** analyzed chronic in vivo recordings acquired after several days during invasive monitoring. These recordings presented substantially greater challenges, including waveform drift, changes in recording stability, overlapping spike templates and larger biological variability between recording sessions. As a result, a more comprehensive post-processing workflow was required: automated spike sorting in kilosort4 (92) was followed by extensive expert-guided quality assessment using a custom graphical user interface, SpikeWise, developed during this work, which integrates multiple visualization and quality control https:

3.5.1 SpikeWise: a graphical user interface for spike sorting postprocessing

To improve the reproducibility and efficiency of spike sorting curation, an open-source graphical user interface, SpikeWise, was developed as part of this thesis and is freely available at **https://github.com/rekabod/spikewise**. The software was designed to provide an intuitive environment for visualization, evaluation and manual refinement of spike-sorting results generated by contemporary automated algorithms.

SpikeWise automatically imports extracellular recordings together with spike timestamps, cluster assignments and associated metadata. When metadata files are incomplete or absent, the software generates the minimal required file structure, allowing immediate inspection and subsequent annotation without interrupting the analysis workflow. The interface integrates broadband recordings, averaged and individual spike waveforms, temporal spike distributions and cluster metadata within a unified interactive environment, enabling rapid navigation between recording periods and neuronal clusters. The framework supports all major postprocessing operations required during manual curation (Figure 2). Individual spikes may be added or removed, clusters can be merged or split, and units can be assigned quality labels (e.g., *good* or *noise*). Cluster quality is

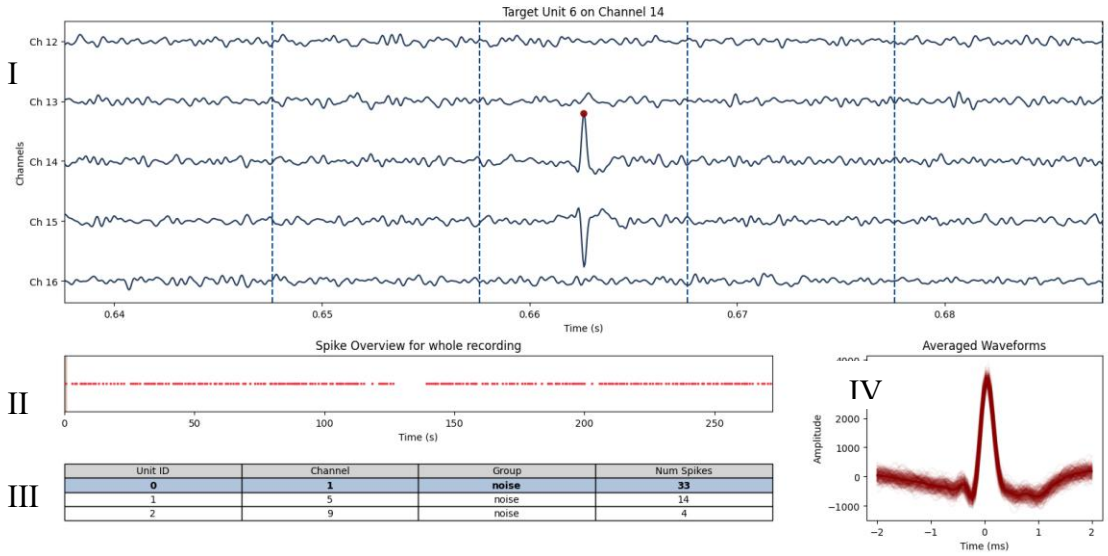


***Figure 2**. SpikeWise graphical user interface, designed for visualizing and editing neural spike data, supporting inspection of spike waveforms, clustering of spike events, and management of spike assignments. The interface main window comprises four components: (I) **main window**, displaying spike waveforms recorded across multiple channels; (II) **overview panel**, providing a global view of spike times throughout the entire recording session; (III) **cluster information table**, summarizing key properties of all detected clusters; and (IV) **waveform view**, showing both averaged and individual spike waveforms for selected units. SpikeViewer is an interactive application designed for visualizing and editing neural spike data, supporting inspection of spike waveforms, clustering of spike events, and management of spike assignments across different neuronal units.*

evaluated using complementary information including waveform morphology, refractory-period violations, temporal stability, autocorrelograms and additional metadata. Interactive visualization and real-time updating of cluster statistics facilitate consistent expert evaluation throughout the curation process. All editing operations are reversible, and curated spike assignments together with updated metadata can be exported directly for subsequent electrophysiological analyses. SpikeWise was used for manual curation of all in vivo and in vitro recordings presented in the **Preprint**, delivering a standardized and reproducible post-processing workflow across the complete dataset. Although originally developed for this work, the software is platform-independent and compatible with outputs from commonly used spike-sorting pipelines.

3.6 Standard electrophysiological signal processing

Following spike sorting and manual curation, downstream electrophysiological analyses were performed on the simultaneously recorded local field potentials (LFPs) and single-unit activity. LFPs provided information on synchronized synaptic activity at the population level, whereas extracellular spike trains were considered as the output of

individual neurons. These complementary ranges of extracellular electrophysiological recordings enabled investigation of neuronal firing properties, oscillatory synchronization and functional interactions across cortical layers and experimental conditions.

3.6.1 Local field potential preprocessing

Prior to analysis, recordings were visually inspected and segments containing electrical artifacts or movement-related noise were excluded. Recordings were additionally processed to remove line-noise contamination and other acquisition-specific artifacts. For the reason that in vivo and in vitro datasets differed in recording conditions, preprocessing pipelines were adapted accordingly. For **Article II**, spontaneous population activity (SPA) events were detected from the local field potential gradient (LFPg, Figure **3**A), following previously established laboratory protocols, described in (113). Individual SPA events were aligned to their amplitude absolute peaks, which served as time zero for event-related averaging. Baseline correction was applied between -150 and -50 ms before the event peak, and averaged LFPg and multiunit activity traces were calculated and analyzed separately for supragranular, granular and infragranular layers. For the analyses presented in the **Preprint**, local field potentials were examined during continuous recordings obtained under resting wakefulness, NREM sleep, and in vitro conditions. In the in vitro state, putative SPA events were identified, and intervals containing dense population activity were excluded to ensure that assessments of theta-range oscillatory features (4–8 Hz) reflected only the underlying background rhythmic activity. Further spectral decomposition and oscillatory analyses were performed following band-specific filtering and interval selection criteria are presented in detail in the relevant subchapter.

3.6.2 Current source density analysis

Concerning the estimation of transmembrane currents' laminar distribution on underlying extracellular field potentials, current source density (CSD) analysis was performed on SPA events of **Article II** and gamma-rich intervals in the data employed for the **Preprint**. CSD is defined as the second spatial derivative of the local field potential and was calculated as the first (one additional spatial derivative of the LFPg signal), recorded across neighboring electrode contacts (55), thereby reducing the influence of distant volume-conducted signals and emphasizing locally generated synaptic currents. Current sinks were interpreted as regions of net inward transmembrane current, generally associated with excitatory synaptic activation, whereas current sources reflected outward

current flow. Derived from CSD analysis of the **Preprint**, the Integrated Sink Strength (ISS) was computed to identify the laminar generators of spontaneous gamma oscillations and to compare their spatial organization between wakefulness, NREM sleep and isolated cortical tissue (**Figure 9**g). The ISS maps only the positive components of the CSD matrix, to prevent source-sink cancellation effects, and computational details are provided in the **Preprint**.

3.6.3 Single-unit waveform characterization and cell type classification

Following spike sorting and manual curation, individual neurons were characterized according to their extracellular waveform morphology and firing dynamics. For **Article II**, neurons were classified using previously established criteria (130). Briefly, putative principal cells and interneurons were distinguished primarily according to extracellular spike halfwidth. Units with half-widths exceeding 0.4 ms were classified as principal cells, whereas units narrower than 0.2 ms were classified as interneurons. Principal cells were further separated into regular-spiking (RS-PC), intrinsically bursting (IB-PC) and unclassified principal cells according to their autocorrelograms and discharge dynamics.

For the **Preprint**, a more extensive classification procedure was employed. Spike waveform features included peak-to-trough latency, primary and auxiliary halfwidths, waveform symmetry, maximal depolarization and repolarization slopes, and peak-to-trough amplitude ratios. Together with firing statistics and autocorrelogram features, these parameters were used to classify neurons as regular-spiking principal cells (RS-PCs), intrinsically bursting principal cells (IB-PCs), non-fast-spiking (NFS) and fast-spiking (FS) interneurons. The maximal firing-rate threshold separating non-fast-spiking from fast-spiking putative inhibitory cells was at 20.1 Hz, using Gaussian mixture modeling.

Neuronal activity was quantified using mean firing rate, maximal firing rate, inter-spike interval statistics, coefficient of variation of inter-spike intervals (ISI CV) and burstiness indices. Burstiness was defined as the proportion of spikes participating in bursts consisting of at least three spikes occurring within a 20-ms interval (130), in the **Preprint**, the ratio of ISIs under 20 ms reported to total was also determined. For **Article II**, neuronal firing was additionally related to spontaneous population activity by comparing firing rates during baseline (-150 to -50 ms) and peri-event (-50 to +50 ms) windows relative to SPA onset. Units were classified as exhibiting increased, decreased or unchanged activity according to predefined statistical criteria. Granger causality analysis

was further performed to assess predictive relationships between individual neuronal firing and spontaneous population events.

3.7 Oscillatory analyses

3.7.1 Spectral epoch detection

For analyses requiring oscillatory activity, sustained spectral epochs were identified using a conservative multistage detection procedure. Continuous local field potential recordings were converted to floating-point signals and analyzed using Welch power spectral density estimates calculated in 4-s windows with 50% overlap. Fractional power was computed for the delta (0.5-3.5 Hz), theta (4-8 Hz), low-gamma (30-50 Hz) and high-gamma (50-80 Hz) frequency bands by normalizing band-limited power to the total spectral power 0.5-200 Hz. For the sake of transient fluctuation reduction, fractional-power time series were smoothed using a three-point running median filter, and detection thresholds were calibrated from paired wakefulness and sleep recordings. For each frequency band, receiver operating characteristic (ROC) analysis was performed, and thresholds were selected by maximizing Youden's J statistic. When ROC separation proved insufficient, percentile-based thresholds were applied instead, and to minimize channel-specific artifacts, an oscillatory epoch was accepted only when the detection criterion was simultaneously fulfilled on at least six recording channels. Candidate epochs were further refined using the Hilbert envelope of the corresponding band-pass filtered signals to determine transition boundaries, but detailed description of the implementation and threshold optimization procedure is provided in the **Preprint**.

3.7.2 Spike-field coupling

Oscillatory synchronization between single neurons and local neuronal populations was quantified using spike-field coupling analysis. Epochs with suprathreshold power density for the bandpass-filtered frequency ranges of interest were used to calculate single unit action potential instantaneous phases, from the analytic signal following Hilbert transformation. For each clustered neuron, the phase corresponding to every action potential was extracted, and synchronization strength was quantified using the phase-locking value $\mathrm{PLV} = \left|\frac{1}{N}\sum_{k=1}^{N} e^{i\phi_k}\right|$, thus PLV is computed as the average of unit-length complex vectors $e^{i\phi_k}$, where $\phi_k$denotes the oscillatory phase at the k-th spike and $N$is the total number of spikes. PLV values range between 0 (uniform phase distribution) and

1 (perfect phase locking), and the preferred phase was determined from the angle of the mean resultant vector, while its length represented phase concentration. In the Preprint, oscillatory analyses focused on delta, theta, low-gamma and high-gamma frequency bands, ranging as described in 3.7.1. Statistical significance was assessed using both the Rayleigh test and circular-shift permutation testing.

3.8 Functional interactions and network analyses

3.8.1 Putative functional connectivity

Putative functional interactions between simultaneously recorded neurons were contingent to cross-correlogram (CCG) analysis. In **Article II**, crosscorrelograms were calculated using 1-ms bins within ±40-ms windows. A putative interaction was identified when the peak of the histogram exceeded the baseline mean by more than 2 standard deviations and contained at least 20 coincident spikes. CCG peaks occurring within 1-3 ms were interpreted as putative monosynaptic interactions, whereas longer delays were considered polysynaptic. For the **Preprint**, on the other hand, CCGs were calculated over ±50 ms windows using 1-ms bins. Putative excitatory and inhibitory interactions were identified when peaks or troughs within the monosynaptic window (1-5 ms) exceeded baseline activity by at least four standard deviations in addition to surrogate statistics passing the test (**Figure 9**a). It is worth noting that because extracellular recordings cannot establish anatomical synaptic connectivity, these interactions are referred to throughout the thesis as putative functional connections (**Figure 9**a).

3.8.2 Population coupling

Following (67), we introduced the measurement of population coupling, quantifying the degree to which individual neurons co-fluctuated with the surrounding neuronal population. Spike trains were converted to firing-rate time series, and for each neuron the Pearson correlation was calculated between its firing rate and the summed activity of all remaining simultaneously recorded neurons, excluding the neuron itself, expressed as $\mathrm{PC}_i = \mathrm{corr}(r_i,\ R_{-i}),$. This metric provides a measure of how strongly a neuron participates in local ensemble activity and was compared across cortical layers, behavioral states and experimental preparations.

3.8.3 Graph-theoretical analysis

Functional network organization was characterized using graph-theoretical analyses applied to single-unit recording ensembles. Individual neurons were represented as nodes,

while weighted edges were derived from unit-level coupling measures. For the **Preprint**, separate undirected weighted graphs were constructed from low-gamma PLV (30-50 Hz), high-gamma PLV (50-80 Hz), and population coupling values. For each measure, the edge weight between two distinct units was defined as the product of their individual coupling strengths: $W_{ij}=S_iS_j$, $i\neq j$, where S_i denotes the corresponding unit-level PLV or population-coupling value. Accordingly, edge weights indicated coupling-based affinities between units instead of direct pairwise neuronal connections. Weak edges were excluded using predefined thresholding criteria.

Network organization was quantified at the single-node level using degree, weighted strength, weighted clustering coefficient, and hubness, the latter expressed as the within-recording z-score of node strength. These measures were used to characterize how individual neurons contributed to the coupling-derived network organization and how network topology differed between physiological states and experimental preparations. Detailed graph-construction procedures are provided in the **Preprint**.

3.8.4 Population dimensionality and activity-space structure

Population dimensionality was quantified from the covariance structure of simultaneously recorded neurons, in order to indicate the complexity and independence of population activity patterns. Three complementary measures were calculated: participation ratio, the proportion of variance explained by the first principal component (PC1 variance), and eigenspectrum entropy. The participation ratio (PR) was calculated using all eigenvalues of the population covariance matrix, specifically: $PR = (\sum_{k=1}^{n} \lambda_k)^2 / \sum_{k=1}^{n} \lambda_k^2$, where λ_k denotes the k-th eigenvalue of the covariance matrix and n is the total number of eigenvalues. This metric estimates the effective number of dimensions contributing to population variance, without applying a fixed eigenvalue threshold: higher values indicate a broader distribution of variance, whereas lower values direct towards an activity profile of smaller number of dominant dimensions. Second, the PC1 variance quantified the fraction of total population variance explained by the first principal component, becoming a complementary measure of the dominance of a shared population mode. Finally, the eigenspectrum entropy quantified the distribution of variance across the covariance eigenvalues, pointing to the complexity of the population activity space. Jointly, these measures were used to characterize changes in population dimensionality

and the organization of shared versus independent neuronal activity across wakefulness, NREM sleep and isolated cortical tissue in the **Preprint.**

3.9 Histological analysis

Histological analyses were used to characterize cortical architecture, neuronal and interneuron density, cellular organization, and tissue integrity. Immunostaining was performed as described in (128, 133). In **Article II**, immunohistochemistry was used to assess laminar organization, possible tumor infiltration or dysgenesis, and pyramidal neuron distribution as well. Sections were stained for NeuN and SMI-32, the latter identifying non-phosphorylated neurofilament-positive pyramidal neurons, positively staining cell density was quantified across cortical layers from non-overlapping microscopic fields, using a custom-built image-analysis pipeline, with selected regions additionally evaluated manually for validation. Detailed procedures are described in **Article II**. In the **Preprint**, tissue blocks obtained immediately after resection ("post-in-vivo") and slices collected following electrophysiological recordings ("post-in-vitro") were processed for NeuN and parvalbumin (PV) immunohistochemistry. Neuronal and PV-positive interneuron densities were quantified in predefined supragranular and infragranular regions of interest, while PV staining coverage (% of the region of interest covered by PV-positive dendrites and axons) was additionally assessed. Image analysis was performed with manual interaction using the custom pipeline (https://github.com/rekabod/neu_roi_ranger). Analyses distinguished tissue fixed immediately after resection from tissue fixed following in-vitro recording.

3.10 Minimal analytical mesoscopic model

In search for the putative mechanisms that could account for the dissociation between population coupling and local gamma synchronization observed experimentally, a minimal analytical mesoscopic model was developed in the **Preprint**. The model consisted of 200 neurons distributed within a three-dimensional volume with laminar proportions based on our own empirical histology. Recurrent excitation and inhibition were distance-dependent, while inhibitory connectivity was additionally modulated by a parameter representing PV axonal survival (approximate range estimated from PV coverage), thereby providing a simplified representation of circuit deafferentation following acute cortical isolation. Network activity was modeled as a noise-driven multivariate Ornstein-Uhlenbeck process, with steady-state covariance obtained from the

corresponding continuous Lyapunov equation. Population coupling was calculated from neuronal correlations with the population activity, whereas local gamma synchronization was represented by a resonance component dependent on recurrent excitation-inhibition balance, PV axonal survival, external drive, and observation noise. Six latent parameters describing external drive, recurrent excitation, recurrent inhibition, PV axonal survival, resonance gain, and observation noise were optimized independently for awake, NREM sleep, and in-vitro conditions using differential evolution. Optimization targeted the experimentally measured population coupling and low- and high-gamma PLV. Participation ratio and variance explained by the first principal component were retained as secondary validation measures. A continuous deafferentation trajectory was generated by interpolation between optimized parameter sets, and first-order Sobol sensitivity analysis was used to estimate the contribution of individual parameters to population coupling and gamma phase-locking.

3.11 Statistical analysis

Statistical analyses were selected according to the distribution and structure of each dataset and were performed using Python-based (v. 3.11-14) analysis workflows, relying on the numpy, scipy and statsmodels libraries. Continuous variables were summarized using appropriate measures of central tendency and dispersion, specified below each figure, whereas comparisons between experimental conditions were performed using parametric or non-parametric tests as appropriate, with paired analyses used when measurements originated from the same recording, slice, or patient. All multiple comparisons were controlled using the Benjamini-Hochberg false discovery rate procedure. Significance of spike-field phase locking was assessed using the Rayleigh test together with circular-shift permutation testing. Crosscorrelogram-based interactions were identified using predefined baseline-derived thresholds rather than relying solely on nominal statistical significance. Where multiple neurons or recording epochs were obtained from the same patient, the hierarchical structure of the data was considered when interpreting statistical comparisons. Detailed statistical procedures, including test-specific parameters and correction methods, are provided in **Article II** and the **Preprint.**

4. RESULTS

This chapter follows the structure outlined in the Objectives, presenting the two manuscripts and their general findings separately. A holistic interpretation of all results is then provided in the Discussion chapter.

4.1 Structural and functional organization of excitatory microcircuits in the human epileptic neocortex

4.1.1 Spontaneous population activity in epileptic and non-epileptic neocortex

Spontaneous population activity (SPA), defined as the same cluster of recurrent SPA events, was observed in both epileptic and non-epileptic human neocortical slices. SPA occurred in 20/40 slices from non-epileptic patients and 20/35 slices from patients with pharmacoresistant epilepsy (Figure **3**A). Individual SPA events consisted of a population burst, characterized by a transient local field potential gradient (LFPg, 1-30 Hz bandpassed), and by an elevated multi-unit activity (MUA, above 500 Hz) component. Consistent with previous observations, SPA could originate from different cortical laminae and was classified according to its spatial extent as supragranular, supragranular–granular, granular, granular–infragranular, infragranular, or translaminar activity. Numerically, 30 different trains of SPA were identified in non-epileptic tissue and 28 in epileptic tissue. Most originated within the supragranular layers (22/30 for non-epileptic and 23/28 in epileptic), while multiple spatially distinct or simultaneous SPAs were observed in several slices. The recurrence characteristics of SPA were comparable between groups, non-epileptic being 0.97 [0.71–1.46] Hz and 1.02 [0.80–1.63] Hz, for the epileptic group (expressed in median, IQR). Neither LFPg nor MUA amplitudes differed significantly between groups (Mann-Whitney U test, $p>0.05$) thus, despite the different pathological backgrounds of the tissue, the basic spectral and recurrence properties of spontaneous population activity were largely preserved in epileptic neocortex.

4.1.2 Glutamatergic contribution to spontaneous population activity

Next, we asked whether excitatory neurotransmission contributed differently to SPA generation in epileptic and non-epileptic tissue: NMDA and AMPA/kainate glutamate receptors were sequentially blocked in slices exhibiting stable spontaneous activity (Figure **3**B). Application of the NMDA receptor antagonist APV (50 μM) significantly

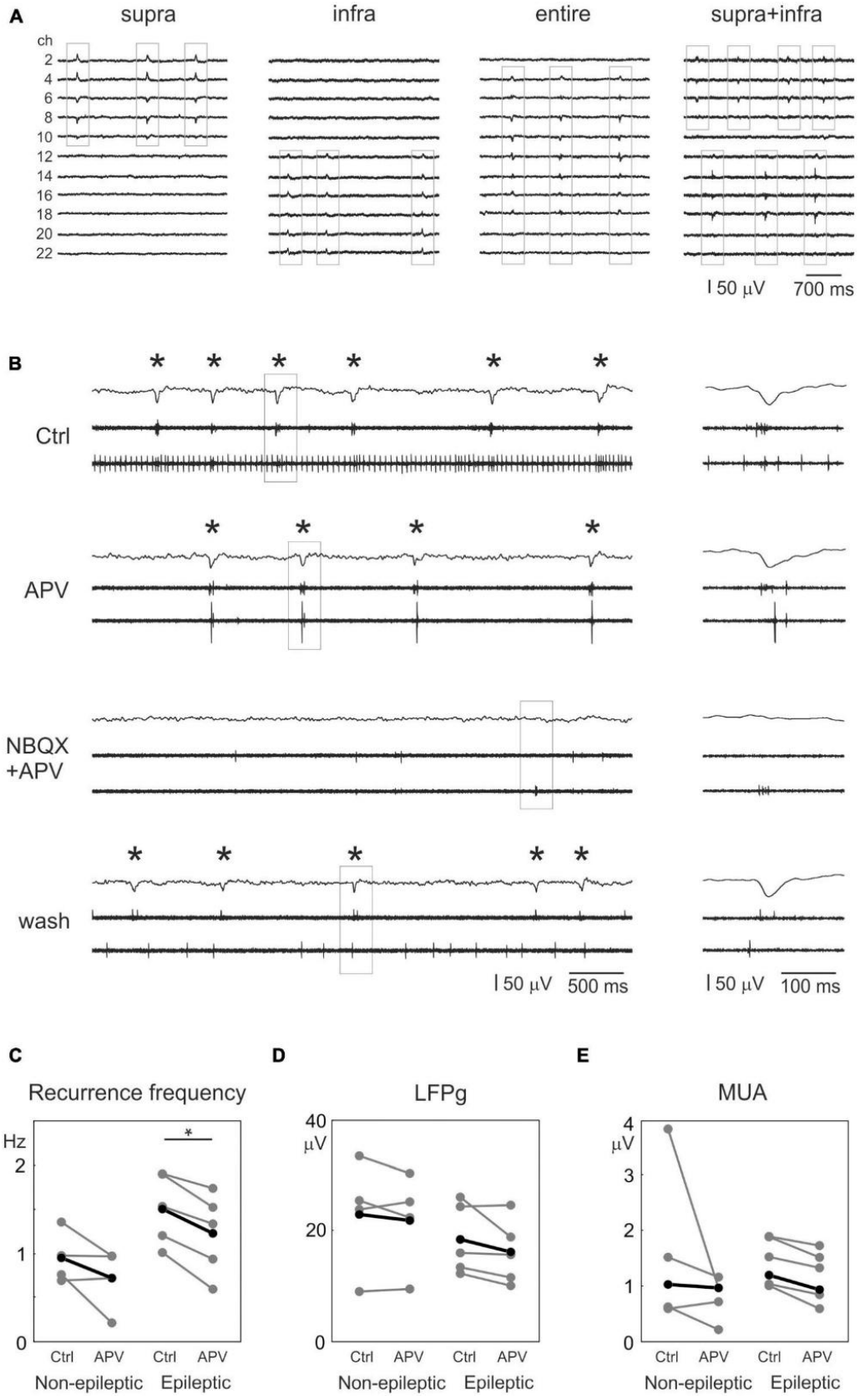


Figure 3 Role of glutamate receptors in the generation of spontaneous synchronous population activity. *(A) Representative recordings of spontaneous population activity (SPA) originating from different layers of human neocortical slices. (B) SPAs and simultaneous single-unit activities recorded from a neocortical slice*

*from a non-epileptic patient during sequential application of physiological solution (control), the NMDA receptor antagonist APV, combined APV+NBQX (NMDA and AMPA/kainate receptor antagonists), and finally physiological solution (washout). Local field potential gradients (LFPg; 1-30 Hz filtered traces) are shown in the upper panels, while the lower panels display single-cell action potentials after high-pass filtering at 500 Hz. Asterisks mark the occurrence of SPAs. Note the reduced presence of SPAs during APV perfusion, and their complete suppression (though not of all action potentials) when NBQX is co-applied. SPAs reappear following washout of the pharmacological agents. Framed sections are shown in detail on the right. (C–E) Statistical comparisons between control conditions and APV application for (C) SPA recurrence frequency, (D) LFPg amplitudes, and (E) multi-unit activity (MUA) amplitudes. The recurrence frequency of SPA significantly decreased in epileptic tissue upon APV application (*p < 0.05). Content reproduced from (128), under CC-BY-4.0.*

reduced SPA recurrence frequency in epileptic tissue (Figure **3**C), while a reduction that did not reach statistical significance was also observed in the non-epileptic tissue. Other SPA parameters, including LFPg and MUA amplitude, were not significantly altered by APV. Subsequent co-application of APV and the AMPA/kainate receptor antagonist NBQX (5 μM) abolished spontaneous population activity in both groups. Following washout, SPA re-emerged, although recovery of the original recurrence frequency was incomplete in some recordings. These findings suggest that AMPA/kainate receptor-mediated transmission is required for the generation of SPA in human neocortical slices, whereas NMDA receptor-mediated transmission makes a significantly greater contribution to spontaneous population activity in epileptic than in non-epileptic tissue.

4.1.3 Single-neuron firing properties and cell-type composition

Single-unit activity was analyzed in recordings obtained during pharmacological manipulation of glutamatergic transmission. In total, 30 neurons from non-epileptic tissue and 34 neurons from epileptic tissue were clustered. Non-epileptic recordings contained 20 putative principal cells (PCs, 60%), 3 interneurons (INs, 10%), and 10 unclassified units (UCs, 30%), whereas epileptic recordings contained 16 PCs (47%), 10 INs (29%), and 8 UCs (24%) (**Figure 4**A-C). Neuronal firing was dynamically affected by glutamate receptor blockade. Only 5 neurons in non-epileptic tissue (16.7%) and 8 in epileptic tissue (23.5%) remained spontaneously active throughout control, APV, and combined APV+NBQX conditions (**Figure 4**D, Figure 5A-C). Conversely, neurons that were silent during control conditions could become active following receptor blockade. This effect was particularly visible among interneurons in epileptic tissue, several of which became active only during combined AMPA/kainate and NMDA receptor blockade. Mean firing rates were not significantly altered by pharmacological manipulation when all recorded neurons or principal-cell and interneuron populations were considered. Firing rates in

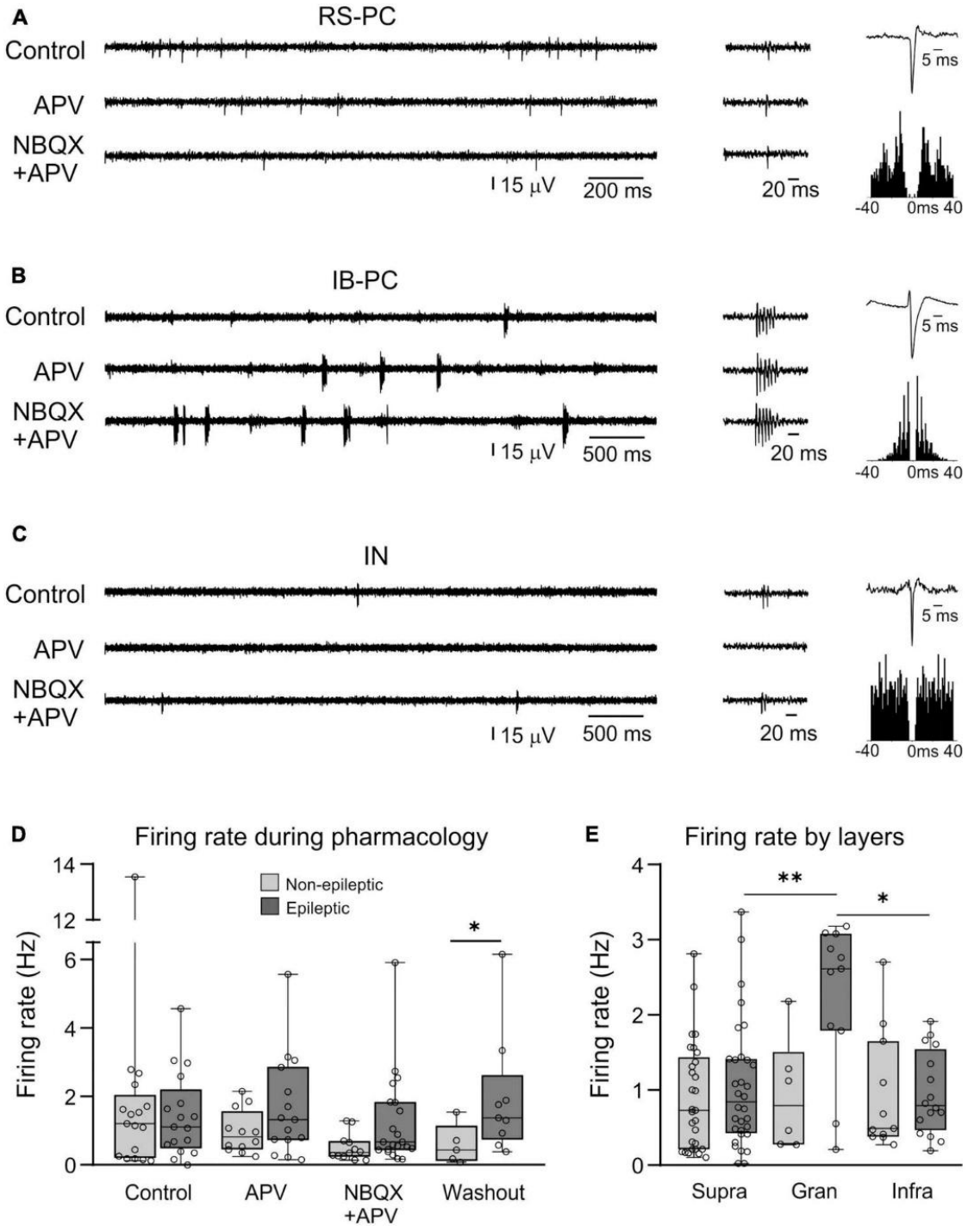


Figure 4. Single-unit firing patterns attributed to distinct neuronal cell types during pharmacological experiments*. Left panels illustrate the firing patterns of (A) regularly spiking principal cells (RS-PCs), (B) intrinsically bursting principal cells (IB-PCs), and (C) interneurons (INs). Middle panels display magnified single-unit traces, while right panels present the corresponding average action-potential waveforms and autocorrelograms. (D) Changes in firing rates of all recorded cells (non-epileptic vs. epileptic) during pharmacological manipulations. (E) Firing rates of cells located in the supragranular, granular, and infragranular layers of the neocortex (*p < 0.05; **p<0.01). Content under terms of CC-BY-4.0 from (128)*

control conditions were comparable between groups (mean±SEM, non-epileptic: 1.01±0.21 Hz; epileptic: 1.17±0.27 Hz). However, neurons recorded from the granular layer exhibited higher firing rates in epileptic tissue than in non-epileptic tissue (2.21±0.31 vs. 0.91±0.30 Hz, **Figure 4**E). This comparison should be interpreted cautiously, since only seven granular-layer neurons were identified in the epileptic group. Bursting properties, nevertheless, differed between the two tissue groups. Overall burstiness (B%) was higher in epileptic than non-epileptic tissue (0.18±0.06 vs. 0.04±0.02; Dunn's multiple-comparison test, $p=0.015$). Under combined APV+NBQX blockade, intrinsically bursting PCs also showed lower B% in epileptic than non-epileptic tissue ($p<0.01$). These suggest that, despite broadly similar mean firing rates, epileptic cortical neurons altered their temporal firing patterns, mirrored by increased burstiness.

4.1.4 Neuronal recruitment during spontaneous population activity

Following this, we asked how individual neurons contributed to SPA generation, therefore changes in firing rate were quantified around SPA events. In non-epileptic tissue, 6/17 neurons increased their firing during SPA under control conditions and 5/12 during APV application. In epileptic tissue, 7/16 neurons increased their firing during control conditions and 7/15 during APV. The proportions of neurons showing increased, decreased, or unchanged activity, but also the magnitude of firing rate increases did not differ significantly between groups. However, intrinsically bursting PCs in epileptic tissue displayed substantially larger increases in firing during SPA than their non-epileptic counterparts (4020±2185% vs. 89.16±7.63%, $p=0.0025$). This comparison was based on a small number of cells and was partly influenced by neurons with no baseline firing, for which relative increases became very large. Granger-causality analysis provided exploratory evidence that the activity of some neurons preceded SPA-related population activity. Five of 29 analyzed neurons in non-epileptic tissue and 13 of 31 in epileptic tissue fulfilled the predefined Granger-causality criteria. Overall, however, the proportion of neurons recruited during SPA did not differ significantly between groups.

It is, however, worth mentioning, that neurons whose firing remained unchanged during SPA showed a significant reduction in activity during APV application in epileptic tissue, suggesting that NMDA receptor-dependent transmission contributed to the maintenance of ongoing neuronal activity even when individual neurons were not strongly recruited by SPA events.

4.1.5 Putative functional interaction readouts between neurons

Pairwise crosscorrelograms were calculated to identify short-latency putative functional interactions between simultaneously recorded neurons. Of 698 possible neuronal pairs, 15 fulfilled the predefined criteria for functional interactions, including 10 putative monosynaptic and 5 polysynaptic relationships (Figure 5F-G).

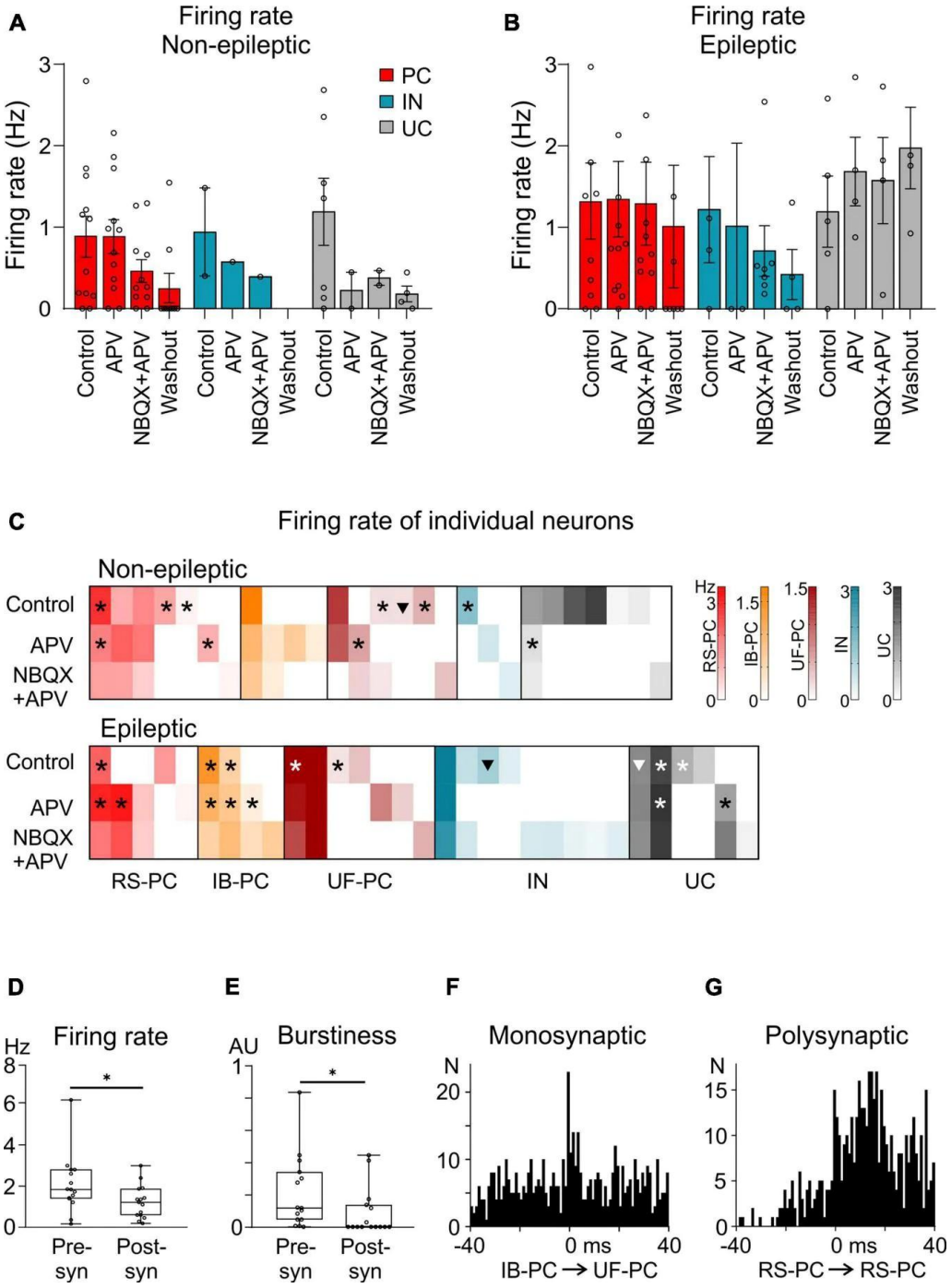


Figure 5. ***Firing-rate dynamics across pharmacological conditions.*** *(A–B) Firing rates of principal cells (PCs), interneurons (INs), and unclassified cells (UCs) under different pharmacological conditions in non-epileptic (A) and epileptic (B) tissue. Firing rates in epileptic samples were not significantly higher*

than in non-epileptic ones. (C) Heatmaps illustrating individual cells' firing rates across conditions (Control, APV, NBQX +APV). Color codes indicate cell-class identity (warm colors for PCs with distinct firing patterns, blue for INs, gray for UCs), while color gradients represent firing-rate magnitude (Hz). Symbols within boxes mark significant rate changes during spontaneous population activity (SPA): asterisks denote increased, triangles decreased firing rates. (D–F) Analyses based on cross-correlograms of reliably connected cell pairs, showing differences in (D) firing rate and (E) burstiness index between presynaptic and postsynaptic members: both significantly different ($p < 0.05$). (F) Example cross-correlogram of a monosynaptic pair, where an IB-PC evokes burst firing in an unidentified principal cell (UF-PC). (G) Example of a polysynaptic connection between two RS-PCs, detected via cross-correlogram analysis. CC BY 4.0 license; reused with attribution (128)

Most identified interactions involved infragranular neurons (11/15), while three occurred between neighboring supragranular and granular channels. All major cell classes participated in the detected interactions, although only one connection involved a PC–IN pair. Notably, intrinsically bursting PCs were overrepresented: 8/15 involved an IB-PC, and in 6 of these cases the IB-PC was the putative presynaptic neuron. IB-PC participation was higher than expected from their representation among recorded neurons (p=0.04, Fisher's exact test). Presynaptic neurons displayed higher firing rates and burstiness than postsynaptic neurons (2.06±0.36 vs. 1.22±0.20 Hz, p=0.045; burstiness 0.20±0.05 vs. 0.08±0.03, p=0.04, Figure 5D-E). Therefore, the limited connectivity dataset suggests a preferential involvement of highly active and intrinsically bursting neurons in the detected functional interactions.

4.1.6 Histological characterization of cortical organization

Histological analysis confirmed the presence of the six-layered neocortical organization in all examined samples (**Figure 6**A-B). Despite the general neuronal loss in epilepsy (133, 134), SMI-32-positive pyramidal neurons were distributed predominantly in layers III, V, and VI, with considerable local heterogeneity in staining density (**Figure 6**C-F). Quantification included 14,034 SMI-32-positive neurons from eight sections obtained from two non-epileptic and three sections from two epileptic samples. SMI-32-positive neuronal density did not differ significantly between groups (51.74±14.93 vs. 46.35±9.98 cells/100 μm³ in non-epileptic and epileptic tissue, respectively, Welch's t-test, p=0.46). Consequently, the density of SMI-32-positive pyramidal neurons was generally preserved in the examined epileptic tissue, despite the functional alterations in glutamatergic signaling and neuronal discharge patterns. Summing up histological aspects, at the structural level, excitatory projection neuron density remained unchanged.

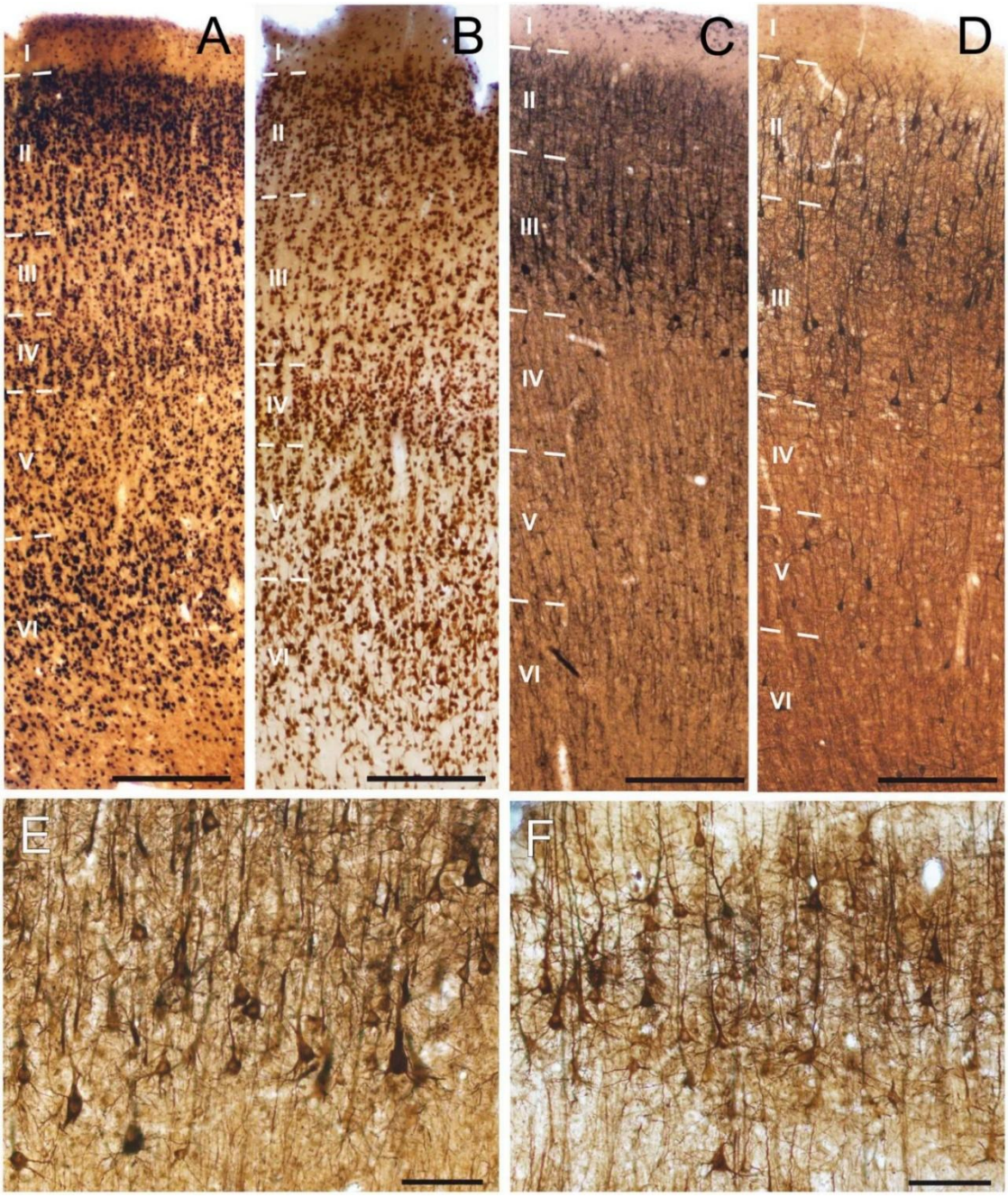


Figure 6. Histological analysis of epileptic and non-epileptic human neocortices*. Neocortical tissue was immunostained for the neuronal marker NeuN in (A) non-epileptic and (B) epileptic samples. SMI-32 staining in both tissue types highlighted projecting pyramidal neurons, either across the full cortical thickness (epileptic, C; non-epileptic, D) or specifically zoomed within layer III (E, F). Although background intensity varied between epileptic and non-epileptic tissue, neuronal density showed no significant difference. All samples were obtained from the temporal lobe. Scale bars: (A–D) 500 µm; (E, F) 100 µm. Adapted from (128), under CC-BY-4.0 license.*

4.1.7 Summary of the findings for Objective 1.

Collectively, these results demonstrate that epilepsy selectively alters the excitatory microcircuit of the human neocortex at multiple organizational levels. NMDA receptor-dependent signaling contributes to the increased recurrence of spontaneous population

activity, whereas AMPA/kainate receptor-mediated transmission is essential for SPA generation irrespective of pathology. Although baseline firing properties of most neuronal classes remain largely preserved, layer IV neurons display enhanced activity in epileptic tissue.

4.2 Functional organization of human neocortical microcircuits in vivo and following experimental isolation

Moving on to Objective 2, we aimed to distinguish contribution of intrinsic local cortical circuitry from that of distributed brain networks, thus electrophysiological activity was compared across matched recordings obtained during wakefulness, NREM sleep, and acute in vitro cortical preparations from the same patients. Laminar local field potentials (LFPs) and single-unit activity were recorded using similar 24-channel microelectrode arrays, allowing comparison of neuronal firing, oscillatory synchronization, functional interactions, population coupling, and laminar activity across physiological states and after surgical isolation of the cortex. In total, 546 well-isolated units were identified across the three experimental conditions and classified as regular-spiking principal cells (RS-PCs), intrinsically bursting principal cells (IB-PCs), non-fast-spiking interneurons (NFS), or fast-spiking interneurons (FS) according to established waveform and firing criteria.

4.2.1 Isolation alters intrinsic excitability while preserving baseline firing

Cortical isolation produced marked changes in extracellular action-potential waveforms. Principal spike halfwidth increased substantially following transition from the intact brain to the in vitro preparation, from a median approximately 0.21 ms in vivo to 0.37 ms in vitro, with the difference remaining significant across putative cell types ($q<10^{-10}$, Figure 7h). Thus, isolation altered the temporal characteristics of extracellular action potentials in both principal cells and interneurons.

Despite these waveform changes, spontaneous baseline firing was broadly preserved across experimental conditions. Mean firing rates showed only modest differences between wakefulness, NREM sleep, and in vitro recordings (Figure 7f). In contrast, the maximal firing rate measured over 1-s intervals increased markedly following isolation, particularly in principal cells, reaching a median of approximately 14 Hz in vitro compared with 6–7 Hz during in vivo recordings ($q<0.0001$, Figure 7g). Measures of firing irregularity and burst propensity showed an overall tendency to increase along the wakefulness-sleep-in vitro axis (Figure 7i-j). NFS interneurons displayed greater firing

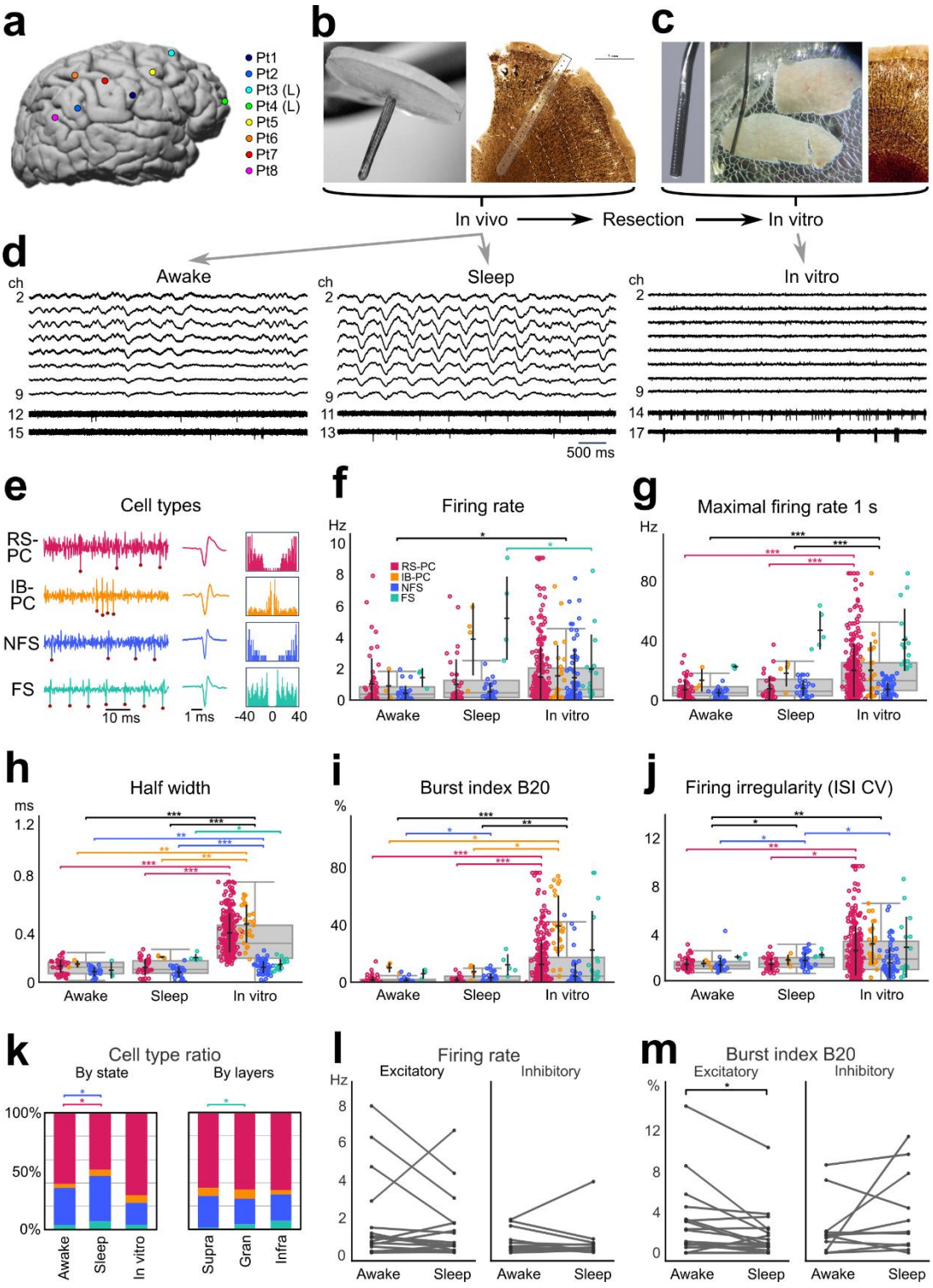


Figure 7 Experimental workflow and isolation-induced shifts in human cortical single-unit electrophysiology. *(a-c) Within-patient experimental framework for tracking identical cortical microcircuits across physiological and isolated states. (A) Representative MR reconstruction illustrating patient-specific laminar microelectrode array locations (Pt1-8), all sites being taken on the right side, if not marked the left hemisphere (L). (b) In vivo configuration of the 24-channel laminar microelectrode, showing the flexible silicone sheet adhered to the electrode shank and pia mater, enabling synchronous electrode–tissue movement (left), alongside histological reconstruction of the electrode track across*

*cortical layers visualized by NeuN staining (right). (c) In vitro electrode architecture (left), acute neocortical slice preparations during recording (middle), and corresponding NeuN-verified laminar architecture (right). (d) Representative broadband (1-500 Hz) local field potentials (top) and high-pass-filtered (>500 Hz) multi-unit traces (bottom) recorded during wakefulness, NREM sleep, and in vitro slice conditions. (e) Electrophysiological classification of single units into regular-spiking principal cells (RS-PCs), intrinsically bursting principal cells (IB-PCs), non-fast-spiking interneurons (NFS), and fast-spiking interneurons (FS), characterized by highpass-filtered traces, aligned spike waveforms, and autocorrelograms. (f-j) Intrinsic single-unit properties across physiological and isolated states. Colors code the different cell types, whereas grey box plots show the total neuronal populations. (f) Baseline firing rates across cell types, showing a global in vivo-to-in vitro increase and elevated FS activity during sleep. (g) Maximal firing rates computed over 1 s windows, revealing sharp elevations in isolated principal cells. (h) Action-potential halfwidths, highlighting narrower interneuron profiles and global wave broadening in vitro. (i) Burst index (B20; proportion of ISIs<20 ms) across states, showing prominent in vitro increases in principal cells and an awake-to-sleep rise in NFS cells. (j) Coefficient of variation of the inter-spike interval (ISI CV), illustrating shifts in spike-train regularity across states. (k) Distribution of cell-type ratios across states, highlighting an awake-to-sleep shift from RS-PCs to NFS cells, with nominal layer-specific (supragranular vs. granular) FS ratio variations. (l-m) Longitudinal tracking of identical single units across wakefulness and NREM sleep (n=42). (l) Pairwise tracking of baseline firing rates showing no uniform state-dependent trajectory. (m) Tracked burst index (B20) trajectories, revealing selective attenuation of burstiness in excitatory populations during sleep, contrasted by stable inhibitory interneuron dynamics. Asterisk legend: * q<0.05, ** q<0.01, *** q<0.001. This figure is employed from the* ***Preprint*** *manuscript.*

irregularity during NREM sleep than during wakefulness, coinciding with changes in the representation of neuronal classes across conditions. RS-PCs were relatively more frequent during wakefulness, whereas NFS neurons became increasingly represented with cortical depth. The availability of repeated recordings from the same neurons provided an additional comparison that was less affected by differences in cell-type composition as 42 units were tracked between wakefulness and NREM sleep. No monotonic change in firing rate was observed across the wakefulness-sleep-in vitro sequence for either putative excitatory or inhibitory populations, but burstiness of the tracked excitatory neurons was significantly reduced during NREM sleep compared with wakefulness (Figure 7l-m). Everything considered, cortical isolation did not simply suppress neuronal activity, but more subtly, it influenced spike waveform and the temporal structure of firing while maintaining substantial spontaneous activity.

4.2.2 Cortical isolation enhances gamma-band spike-field synchronization

The most pronounced functional differences across experimental conditions appeared in how single neurons coupled to ongoing LFP rhythms. Delta-band phase locking was quantified only during NREM sleep, whereas theta-band coupling was assessed exclusively in vitro, with SPA events approximating single-cycle theta omitted from

analysis. Across these bands, locking strength and the proportion of significantly phase-locked neurons varied only modestly between conditions (**Figure 8**a-d, f). In

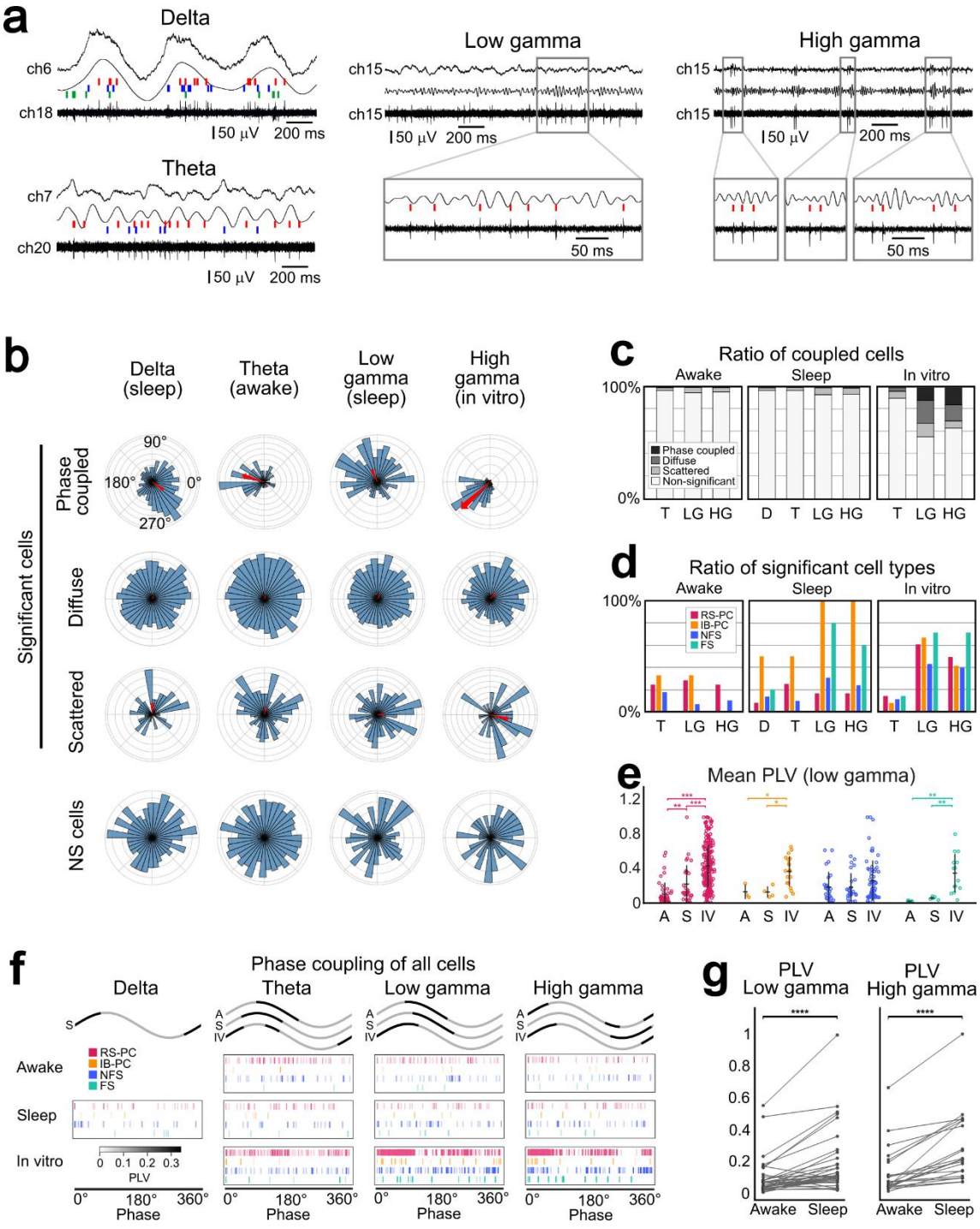


Figure 8 Isolation-induced amplification of cell-type-specific spike–field phase synchronization. *(a) Representative local field potential (LFP) traces band-pass-filtered for delta (1-4 Hz), theta (4-8 Hz), low-gamma (30-50 Hz), and high-gamma (50–80 Hz) oscillations (top), aligned with simultaneous single-unit spike raster plots (bottom). Magnified callouts highlight fine-scale spike alignment relative to individual low- and high-gamma wave cycles. (b) Representative polar histograms illustrating distinct single-unit phase-coupling categories: strongly phase-coupled (highly localized distributions), diffuse (broadly directional distributions), and scattered (uniform but statistically significant distributions),*

contrasted with non-significant cells (NS; failing joint circular and surrogate-shuffled thresholds). Superimposed arrows indicate resultant population vectors, where arrow length denotes the Phase-Locking Value (PLV) and angle denotes the preferred firing phase. (c) Relative proportions of single units classified into different phase-locking topology modes across the recorded population. (d) State-dependent proportions of single units showing statistically significant phase-coupling across frequency bands, demonstrating a robust shift toward high-frequency recruitment in vitro. (e) Mean PLVs for low-gamma (left) and high-gamma (right) bands across states, resolved by functional cell classes. Note the progressive escalation in coupling strength from wakefulness to sleep and its pronounced amplification in vitro across all cell types except non-fast-spiking (NFS) interneurons. (f) Distribution of preferred firing phases for significantly coupled single units, projected onto idealized sinusoidal wave cycles for delta, theta, low-gamma, and high-gamma bands. Circular means are color-coded by state: light gray (awake), dark gray (NREM sleep), and black (in vitro). (g) Pairwise longitudinal tracking of low-gamma and high-gamma PLV magnitudes within identical, robustly isolated single units (n = 42) across the endogenous in vivo wakefulness-to-sleep transition. Error bars represent mean ± s.e.m.; significance markers denote FDR-corrected q values. Figure adapted from the corresponding ***Preprint****.*

contrast, gamma-band synchronization increased progressively from wakefulness to NREM sleep and reached its highest levels in the isolated cortex.

Low-gamma phase-locking value medians showed a trend of 0.075 - 0.120 - 0.369 taking wakefulness, NREM sleep and in vitro as distinct conditions ($q<10^{-4}$, **Figure 8**e). High-gamma phase locking showed a similar progression, increasing from 0.105 to 0.144 and 0.414 on the wakefulness-NREM-in vitro axis ($q<10^{-4}$).

Importantly, recordings from the same neurons demonstrated that the transition from wakefulness to NREM sleep was already associated with a significant increase in both low- and high-gamma phase locking ($q=2.81\times10^{-4}$, **Figure 8**g), indicating that enhanced gamma synchronization was not exclusively a consequence of tissue isolation. The increase in gamma coupling was particularly prominent among FS neurons. In the in vitro condition, clusters assigned to this cell type were approximately five times more likely to exhibit significant gamma coupling, whereas excitatory populations showed an approximately twofold increase.

4.2.3 Enhanced gamma synchrony is accompanied by reduced population coupling and functional network integration

We next tested the link between the increase in oscillatory synchronization and the integration of individual neurons within the local population. Population coupling was calculated from the relationship between the firing rate of each neuron and the activity of the remaining simultaneously recorded population. In contrast to gamma phase locking, population coupling decreased markedly following cortical isolation. Median population

coupling was 0.107 during wakefulness, 0.165 for NREM sleep, and 0.039 in vitro ($q<10^{-4}$), meaning that the isolated cortex exhibited stronger synchronization to local gamma

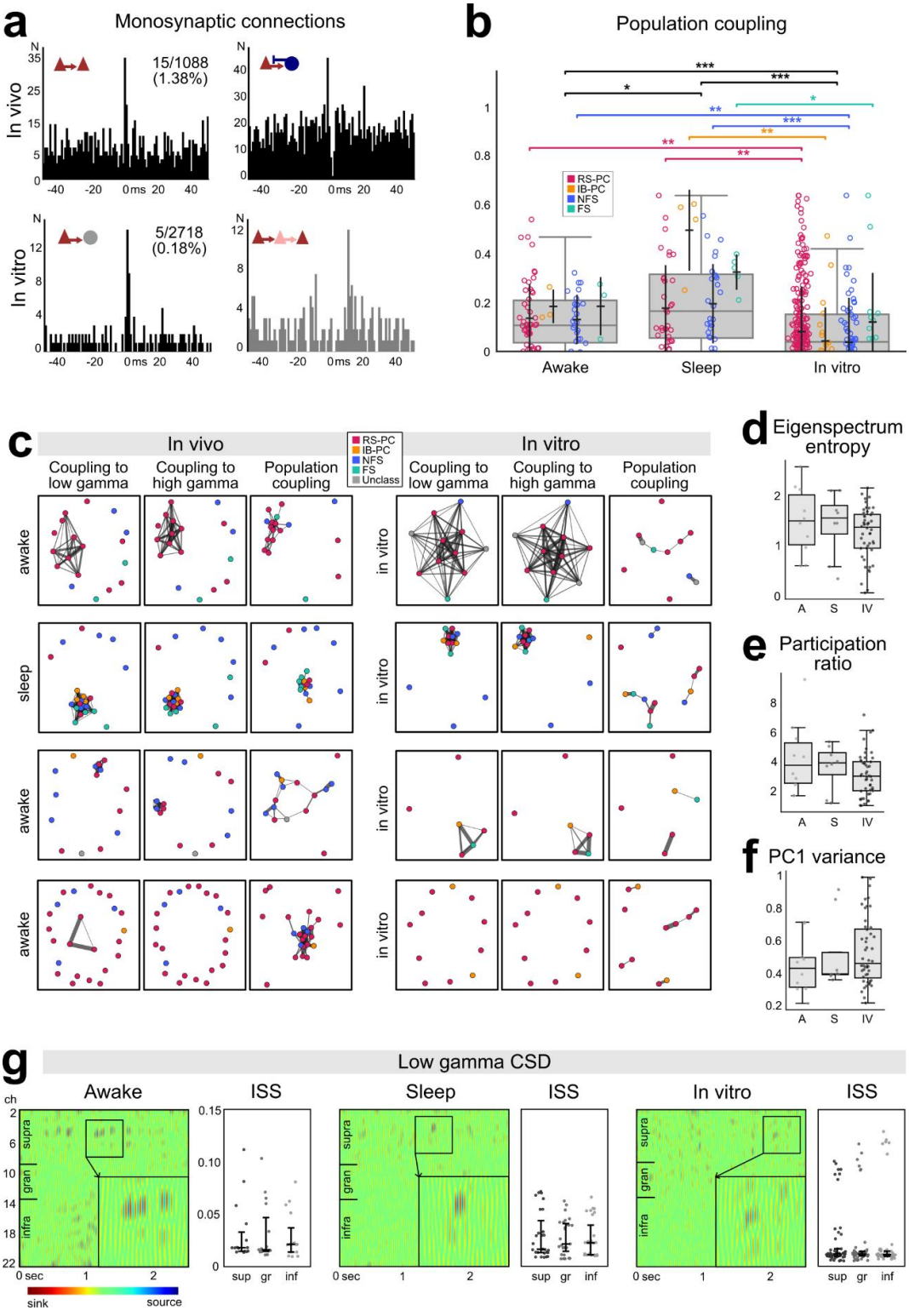


Figure 9. Cortical isolation collapses functional network integration and population dimensionality while preserving local oscillatory dynamics. *(a) Putative monosynaptic and polysynaptic microcircuit interactions. Representative cross-correlograms (CCGs) from simultaneously recorded single units.*

Examples illustrate excitatory monosynaptic connections (PC–PC), simple and feedback excitatory–inhibitory interactions (PC–IN), and delayed polysynaptic interactions. Reported values correspond to statistically significant putative monosynaptic connections relative to the total number of possible synaptic interactions.(b) State- and cell-type-dependent modulation of population coupling across wakefulness, NREM sleep, and in vitro slice preparations, stratified by cell class. Coupling strength shows a global reduction following cortical isolation (NREM > wakefulness > in vitro with Benjamini–Hochberg FDR correction). The collapse is most pronounced in RS-PC and NFS populations, with additional significant reductions observed in IB-PC and FS units between sleep and in vitro conditions. Grey box plots represent the total neuronal population recorded in the given state. (c) Graph-theoretical topology across functional coupling and oscillatory regimes. Network graphs depict pairwise functional relationships derived from low-gamma (30–50 Hz) and high-gamma (50–80 Hz) phase-locking values (PLV) and population coupling. Edge thickness and proximity reflect inter-unit signal similarity and connection strength. Each graph represents a single recording session (N = 8 patients). In vivo states exhibit strong, globally coherent coupling topology, whereas in vitro networks display modular, gamma-dominated clustering. (d-f) Population dimensionality metrics on the wakefulness-sleep-in vitro axis: (d) eigenspectrum entropy of the covariance matrix; (e) network participation ratio; (f) fraction of total variance explained by the first principal component (PC1 variance). These measures reveal a progressive reduction in participation ratio and eigenspectrum entropy, accompanied by an increase in PC1 variance from wakefulness to in vitro, indicating a state-dependent collapse in dynamic dimensionality. (g) Laminar low-gamma current source density (CSD) profiles and sink strength. Representative laminar LFP traces and computed CSD profiles for low-gamma oscillations (30–50 Hz) across wakefulness, NREM sleep, and in vitro slices. Integrated Sink Strength (ISS) quantified across supragranular, granular, and infragranular layers demonstrates preserved spatial generator configurations across all three states. Data are represented as mean ± SEM or individual unit/session trajectories overlaid on boxplots. Significance brackets denote FDR-corrected pairwise comparisons (q<0.05, ** q<0.01, *** q<0.001). This image is reused from the* ***Preprint****.*

oscillations despite a substantial reduction to which individual neurons participated in population-wide activity (**Figure 9**b). Putative functional interactions between simultaneously recorded neurons showed a similar reduction: pairwise crosscorrelogram analysis identified putative monosynaptic interactions in 1.38% of tested pairs in vivo (15/1088), compared with only 0.18% of pairs in vitro (5/2718, **Figure 9**a). The reduction in detected interactions was therefore disproportionate to the increase in gamma synchronization, indicating that the latter did not represent a generalized strengthening of functional connectivity.

Network-level analysis further demonstrated that gamma synchronization and structural integration represented distinct properties of the in vivo cortical network. In awake recordings, gamma-network closeness and node degree were strongly negatively correlated (r= -0.94), indicating that neurons with strong gamma coupling tended to occupy relatively peripheral positions within the functional network. Rather than forming a single highly integrated gamma-synchronized core, the awake and NREM sleep gamma network graphs, illustrated as in Figure 9c, were therefore organized into partially segregated functional clusters. On the other hand, when population coupling of neuron

clusters belonging to given recordings were represented in the same graphwise fashion, in vivo neural populations showed more cohesive functional network architecture. Similarly, dimensionality analyses like eigenspectrum entropy, participation ratio and PC1 variance revealed that neuronal population activity occupied a substantially lower-dimensional state space in vitro, indicating that experimentally isolated cortical networks express a reduced repertoire of activity patterns (Figure 9d-f).

We also wanted to check whether in the increased spike-LFP synchronization is linked to a stronger laminar transmembrane current generation. Therefore, current source density (CSD) was also quantified across cortical layers. High-gamma sink-source organization remained comparatively stable across wakefulness, NREM sleep, and in vitro conditions, with no significant differences in layer-specific integrated sink strength. In contrast, low-gamma sink strength was significantly reduced in vitro despite the marked increase in single-unit phase locking (Figure 9g). As a result, enhanced gamma synchronization in the isolated cortex was not accompanied by a proportional increase in bulk laminar current generation.

Together, these findings outline a dissociation between two aspects of cortical coordination. Cortical isolation reduced broad population integration and putative neuronal interactions while simultaneously increasing spike-gamma synchronization along with preserved or reduced gamma CSD profiles. These results suggest that the isolated microcircuit shifted towards an activity characterized by strong local rhythmic coordination but weak participation in the activity of the wider neuronal population.

4.2.4 Histological preservation and dissociation of structure-function relationships

Next, we hypothesized that the asserted physiological changes associated with isolation could theoretically reflect nonspecific deterioration of the recorded tissue. In an attempt to distinguish functional reorganization from major structural loss, neuronal (NeuN) and inhibitory markers (parvalbumin) were quantified in histological samples obtained either immediately after surgical resection or after completion of the acute in vitro recordings. NeuN-positive neuronal density retained the expected laminar organization, with significantly higher density in supragranular than infragranular cortex (1241 vs. 750 cells mm^{-2}, $q=7.14\times10^{-24}$, **Figure 10**a). Notably, overall neuronal density was essentially unchanged between tissue processed immediately after resection (“post-in-vivo”) and tissue fixed following electrophysiological recording (“post-in-vitro”), with both groups

showing an average density of ~985 cells mm^{-2} (q=0.98). Accordingly, the substantial physiological reorganization observed after isolation occurred without detectable loss of the overall neuronal population.

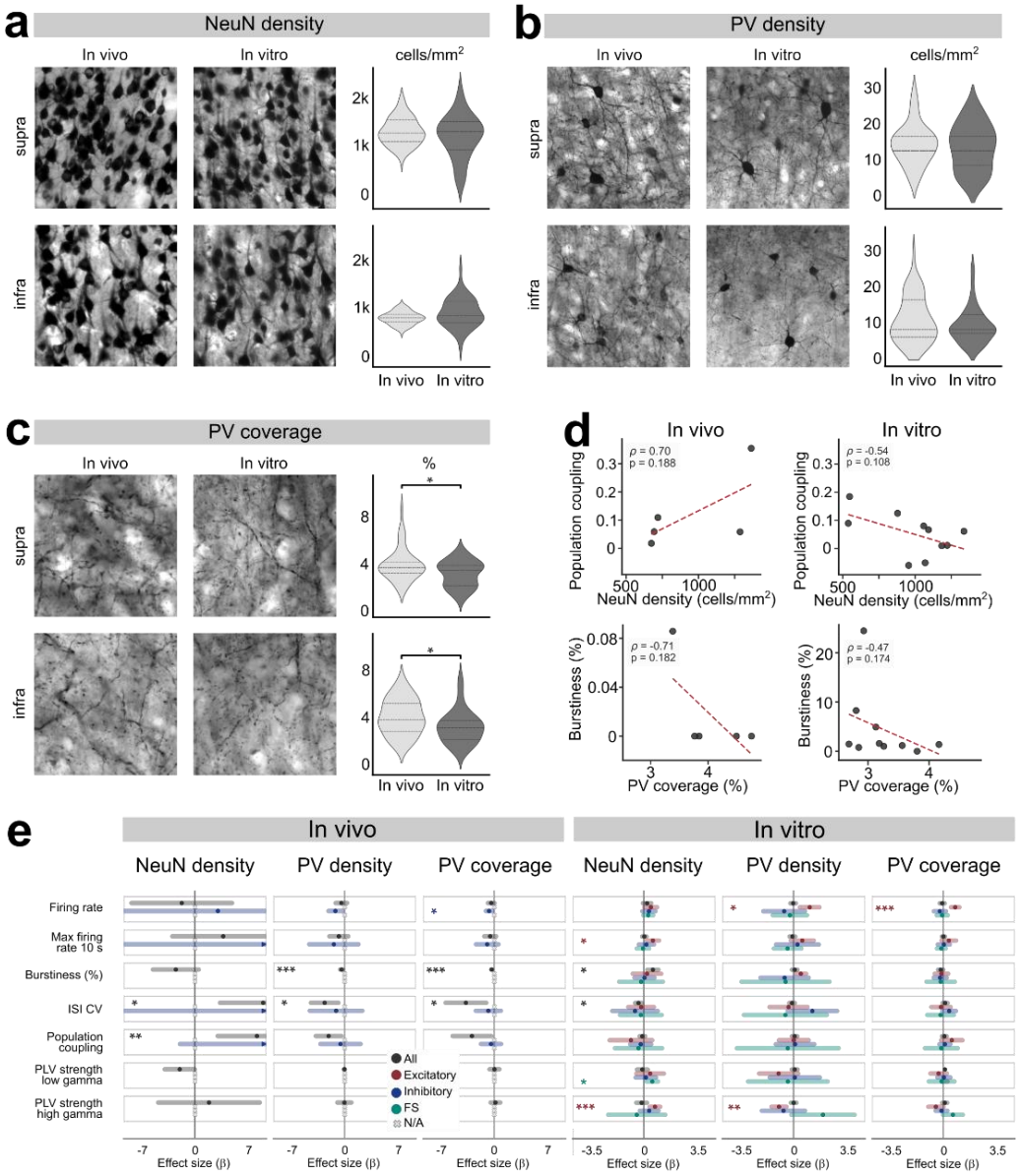


Figure 10. Structural preservation and state-dependent decoupling of histological properties from functional integration. *(a–c) Representative supragranular and infragranular light micrographs from tissue fixed immediately after resection (in vivo) and following acute slice electrophysiology (in vitro). (a)* ***NeuN-based neuronal density:*** *ROIs (300 × 300 µm²) showing preserved laminar density profiles across conditions, with consistently higher supragranular density. (b)* ***PV-positive interneuron density:*** *ROIs (500 × 500 µm²) demonstrating stable interneuron counts following isolation. (c)* ***PV coverage*** *(neuropil integrity)****:*** *ROIs (500 × 500 µm²) showing modest but significant post-isolation reductions in PV process coverage within both supragranular and infragranular cortex. (d) Structure-function relationships****:*** *Spearman correlations comparing NeuN density (cells/mm²) with single-unit population coupling (top) and PV coverage (%) with single-unit burstiness (bottom) in vivo and in vitro. In vivo NeuN density positively*

*predicts coupling (ρ = 0.70), whereas this relationship reverses after isolation. PV coverage and burstiness (%) inversely correlate in both states, with stronger coupling in vivo. (e) Mixed-effects modeling of histological predictors: Standardized regression coefficients (β ± 95% CI) from linear mixed-effects models (nested patient and session random effects) quantifying the influence of NeuN density, PV density, and PV coverage on single-unit metrics. NeuN density robustly predicts population coupling in vivo, but this relationship collapses and inverts in vitro. Multiple comparisons are FDR-corrected (q-values; * q<0.05, **q<0.01, *** q<0.001). Content reused from the* ***Preprint****.*

PV-positive interneuron density similarly showed no significant difference between the corresponding tissue conditions across cortical layers (**Figure 10**b). PV-positive process coverage (% of area occupied by PV+ dendrites and axons), however, was modestly reduced following in vitro recording, from 3.83% to 3.08% in supragranular cortex (q=0.040) and from 4.30% to 3.45% in infragranular cortex (q=0.0017, **Figure 10**c). These findings were interpreted as a preservation of the major cellular components of the cortical microcircuit, accompanied by a more subtle alteration of inhibitory neuropil.

We next examined the correlation between local architecture features and their relationship to functional network organization. Along with Spearman correlation plots suggesting a tendency in histology-electrophysiology metric particularities (**Figure 10**d), we continued with mixed-effects modeling to test whether histology markers can act as predictors on the electrophysiological readouts of the same site of investigation.

We found that in the intact brain, neuronal density was a strong positive predictor of population coupling in (standardized $\beta=7.76$, $q=8.18\times10^{-253}$, **Figure 10**e), namely, regions containing a greater density of neurons exhibited stronger integration of individual neurons into ongoing population activity. PV-related measures were also associated with neuronal firing and burst generation, consistent with a contribution of local inhibitory architecture to the regulation of excitability.

The relationship between structure and function changed substantially following isolation. The positive association between neuronal density and population coupling observed in vivo was weakened and reversed in vitro. Congruently, the rank correlation between NeuN density and population coupling changed from positive in vivo ($\rho=0.70$) to negative in vitro ($\rho=-0.54$), although neither correlation reached significance when considered separately, out of the limited number of histological samples. Similar weakening of structure-function relationships was observed for PV-related measures and burst dynamics. To that end, the electrophysiological reorganization following isolation

was not primarily attributable to neuronal loss. Instead, cortical isolation reversed the relationship between anatomical architecture and functional network integration.

4.2.5 A minimal mesoscopic model reproduces the dissociation between population coupling and gamma synchronization

As a last milestone, we wanted to explore the opposing changes in population coupling and gamma synchronization, asking if this seemingly paradoxical phenomenon could arise from a limited set of circuit-level mechanisms.

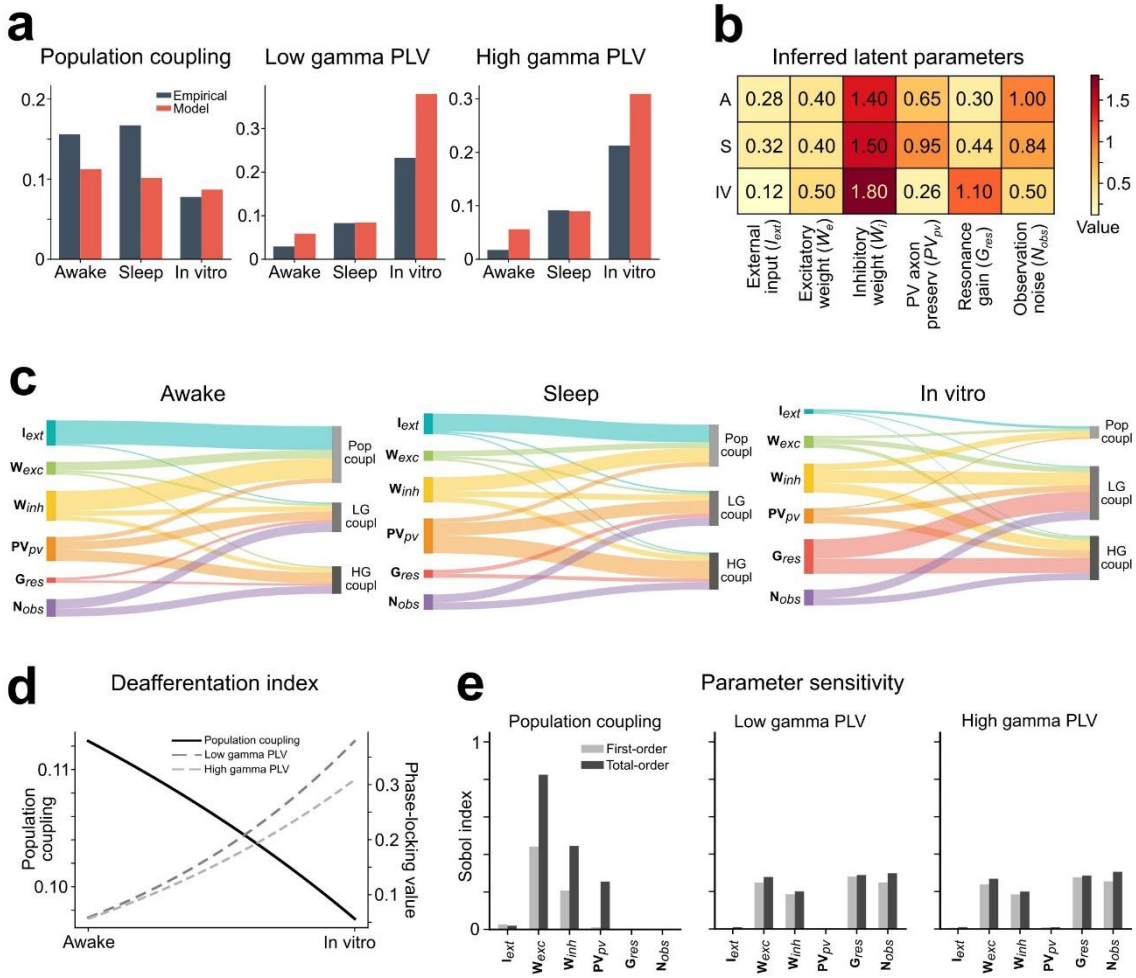


Figure 11. Minimal mechanistic account of the population coupling/gamma phase coupling paradox. *(a) Comparison of empirical (dark) and model (red) population coupling and gamma phase locking values. (b) Optimized latent parameters reveal loss of external drive and PV axonal survival accompanied by increased resonance gain along the wakefulness-sleep-in vitro axis. (c) Sankey decomposition of latent-parameter contributions, ribbon width reflects mechanistic influence on each observable. (d) Model trajectory under continuous interpolation from the awake to the in vitro parameter set. (e) Sobol sensitivity indices demonstrate dissociation between parameters governing population coupling and those controlling gamma synchrony. This figure is reproduced from the* ***Preprint.***

As an attempt to answer, a minimal analytical mesoscopic model was developed, which incorporated recurrent excitation and inhibition, external drive, preservation of parvalbumin-associated axonal connectivity, local resonance gain (representing the strength of intrinsic gamma-frequency amplification within the circuit), and observation noise as six interpretable parameters. The model was fitted independently to the awake, sleep, and in vitro conditions using population coupling and low- and high-gamma phase-locking as the primary empirical targets. The model reproduced the central experimental dissociation: population coupling decreased progressively from wakefulness to NREM sleep and in vitro, whereas both low- and high-gamma phase locking increased along the same trajectory. Model predictions reproduced the empirical population-coupling values with deviations of approximately 28% in the awake condition and 12% in vitro (**Figure 11**a).

Parameter optimization identified distinct mechanisms underlying the two functional dimensions. External drive was progressively reduced along the wakefulness-sleep-in vitro trajectory, accompanied by reduced PV axonal preservation (see also changes in PV coverage) and an increase in local resonance gain (**Figure 11**b). Sensitivity analysis further indicated that external drive was the dominant determinant of population coupling, whereas resonance gain and PV axonal preservation exerted the strongest influence on gamma phase locking (**Figure 11**c). Continuous interpolation between the optimized awake and in vitro parameter sets produced a gradual decline in population coupling, going hand in hand with a monotonic increase in low- and high-gamma synchronization (Figure 11d-e). These results indicate that the two apparently opposing consequences of cortical isolation can arise from partially dissociable circuit mechanisms: reduction of distributed external drive decreases population-wide integration, whereas altered local inhibitory architecture and enhanced resonance endorse gamma-band synchronization.

4.2.6. Summary of the findings for Objective 2

Throughout the matched datasets in vivo and in vitro recordings, cortical isolation produced a measurable reorganization of human cortical dynamics. Spontaneous firing remained comparable across the different contexts of investigation, although action-potential waveforms and maximal firing output were changed. At the network level, in vitro measurement circumstances markedly reduced population coupling and putative neuronal interactions, while simultaneously increased gamma-band spike-field

synchronization, particularly among FS neurons. Laminar CSD demonstrated that this increase in spike-field coupling was not accompanied by a corresponding increase in gamma-frequency transmembrane current generation.

Histological analyses confirmed that these functional changes occurred despite the preservation of overall neuronal density and PV-positive interneuron density, though with modest changes in PV coverage. Despite these, isolation weakened the relationship between cortical architecture and functional integration, highlighting that the embedding of local circuits within distributed brain networks is essential for translating anatomical organization into population-level dynamics. Finally, the mesoscopic model demonstrated that reduced external drive and altered local inhibitory/resonant mechanisms can majorly account for the opposing changes in population coupling and gamma synchronization.

Taken together, these findings indicate that isolated human cortical microcircuits do not behave as autonomous versions of their in vivo counterparts. Removal from the intact brain preserves substantial local neuronal activity but fundamentally reorganizes its coordination: broad population integration is reduced, whereas local gamma synchrony becomes disproportionately strong. The in vitro state therefore represents a distinct dynamical regime in which intrinsic cortical mechanisms become uncoupled from the distributed network context that normally constrains their activity.

5. DISCUSSION

The present thesis investigated human neocortical organization across cellular, local-circuit and distributed network scales. Two complementary experimental approaches were combined: pharmacological and electrophysiological characterization of human neocortical microcircuits in epileptic and non-epileptic tissue, and matched recordings from the intact human brain and acute cortical slices, that were ultimately complemented by histological assessment. Together, these experiments address two related questions, with slightly different experimental frameworks: how intrinsic cortical circuitry generates coordinated activity, with a special regard to the excitatory machinery, and how embedding within the intact brain modifies these locally generated dynamics.

5.1 Excitatory microcircuits and their reorganization in epilepsy

The first objective was to determine how excitatory neurotransmission and local circuit organization contribute to spontaneous activity in the human neocortex, and outline how these mechanisms are altered in pharmacoresistant epilepsy. Our results support the view that human cortical microcircuits possess a substantial intrinsic capacity for recurrent activity. Spontaneous population activity persisted in isolated slices from both epileptic and non-epileptic tissue, revealing that its generation does not require ongoing interaction with distant cortical or subcortical structures. This is consistent with previous observations of spontaneous population activity in cortical slices (113, 129, 130, 135, 136).

The pharmacological experiments further identify fast glutamatergic transmission as a critical substrate of this intrinsic activity. AMPA/kainate receptor blockade abolished spontaneous population activity in both tissue groups, whereas NMDA receptor blockade significantly reduced recurrence in epileptic tissue and showed a similar trend in non-epileptic tissue - indicating a role for NMDA receptor-dependent mechanisms in spontaneous activity across both tissue types. However, the present data do not reveal whether this contribution differs between groups. The observed effects were primarily expressed at the population level rather than as generalized increases in single-neuron firing.

Subsequently, these effects were expressed predominantly at the population level rather than as a generalized increase in single-neuron firing. Mean firing rates changed relatively little during glutamate receptor blockade, whereas the occurrence of coordinated population events was strongly affected. Similarly, the epileptic tissue showed increased

burstiness and higher firing rates in granular-layer recordings without evidence for a uniform increase in neuronal excitability. These observations support a network-level interpretation of epileptic dysfunction, in which altered temporal coordination and recurrent synaptic interactions may be more important than a simple elevation of intrinsic firing propensity (137).

The putative connectivity analysis provides additional evidence for selective circuit organization. Although only a small number of functional interactions could be identified, intrinsically bursting principal cells were disproportionately represented among detected connections and frequently occupied the presynaptic position. This observation is compatible with the proposed role of bursting pyramidal neurons as powerful drivers of local cortical activity, although the small number of detected connections requires cautious interpretation (130, 138).

Histological findings do likewise argue against widespread loss of the principal excitatory neuronal population as the primary explanation for the observed functional differences. SMI-32-positive pyramidal-cell density did not differ significantly between epileptic and non-epileptic samples, despite the presence of dysgenetic or structurally altered tissue in individual cases. Thus, the epileptic cortex appears to retain the overall density of long-projecting excitatory cells of the neocortical microcircuit, while operating under altered excitatory and network conditions (139).

Taken together, these findings suggest that epilepsy modifies the functional wiring of an otherwise structurally preserved cortical microcircuit. Although epilepsy is associated with a modest overall neuronal loss (140), long-range projecting pyramidal cells appear largely spared, as supported by SMI-32 staining in the present study. At the same time, previous work has shown that excitatory axonal sprouting (well-documented for dentate granule cells (140) and cornu Ammonis pyramidal neurons (141, 142), and also present in the neocortex (140)) can enhance synaptic excitation within local circuits. Our results are consistent with this view: while local excitatory microcircuits in epileptic cortex are altered, they retain the capacity to generate population activity patterns comparable to those observed in non-epileptic tissue. Instead of just merely setting up entirely new dynamics, epilepsy appears to reshape the contribution of specific excitatory mechanisms to intrinsic recurrent activity (143). We found this distinction is critical, as it separates the normal capacity of cortical tissue to generate coordinated activity from the pathological

mechanisms that can increase its persistence, synchronization or susceptibility to abnormal recruitment.

5.2 Local microcircuits versus large-scale network embedding

The second objective addressed a different level of organization: which aspects of cortical dynamics are generated intrinsically by local circuitry and which depend on the intact embedding of the cortex within distributed brain networks. Matched (in vivo) and similar (in vivo-in vitro) recording sites from the same cortical region during wakefulness, NREM sleep and after acute isolation provided a direct comparison between these conditions.

The central finding was a dissociation between local synchronization and network integration. Isolation substantially altered neuronal waveform properties and maximal firing output, but spontaneous baseline firing and cell type-specific firing characteristics remained comparatively stable. In contrast, gamma-band spike-field coupling increased dramatically in vitro. Both low- and high-gamma PLV increased from wakefulness through NREM sleep to the isolated state, with the strongest synchronization observed in vitro. The enhancement was particularly pronounced among putative inhibitory neurons and was strongest in fast-spiking interneurons, consistent with the established role of inhibitory networks in gamma generation (14, 114, 144). This increase in synchrony should not, however, be interpreted as evidence for greater network integration. Population coupling decreased markedly following isolation, and putative monosynaptic interactions became rare. Thus, the isolated cortex became more synchronized locally while simultaneously becoming less functionally integrated. Synchronization describes temporal coordination among participating neurons, whereas integration reflects the extent to which neuronal activity is embedded within a broader network. These properties can therefore change in opposite directions, consistent with theoretical accounts emphasizing a balance between integration and segregation in neural systems (145, 146). The dimensionality measures provide an important complement to this interpretation. The higher PC1 variance, participation ratio and eigenspectrum entropy observed in the intact brain indicate that cortical populations occupy a richer and more diverse activity space than isolated tissue. Reduced dimensionality after isolation is therefore consistent with a transition toward a smaller repertoire of recurrent network states. Such reduced

population diversity may limit computational flexibility even when local neuronal synchronization is high (111, 147)

The CSD analysis further separates oscillation generation from network integration. Laminar high-gamma sink-source organization was preserved across experimental conditions, whereas low-gamma integrated sink strength was reduced in vitro despite the prominent increase in spike-field coupling. Therefore, stronger phase-locking does not necessarily imply stronger overall transmembrane current generation. The isolated network may instead enter a more stereotyped, low-dimensional oscillatory engagement, in which a relatively constrained local circuit produces highly coherent neuronal timing.

The structural data, both ours and previously confirmed in literature reinforce this distinction (148). Overall neuronal density was preserved after in vitro recording, whereas PV process coverage showed a modest reduction. More importantly, the relationship between structure and function changed after isolation. In the intact brain, neuronal density positively predicted population coupling, whereas this relationship was weakened or reversed in isolated tissue. This suggests that local architecture contributes to functional integration when the cortex remains embedded within expanding networks, but becomes a less reliable predictor of functional organization once those long-range interactions are removed. These outcomes therefore challenge a simple interpretation of the slice preparation as merely a reduced version of the intact cortex. Isolation does not simply decrease activity, but it selectively removes long-range inputs and reorganizes the remaining local network, producing a state characterized by preserved intrinsic activity, enhanced local synchrony and reduced population integration (37, 149, 150).

5.3 A unified view: local activity generation and distributed organization

The two objectives converge on a common interpretation of human cortical organization: local recurrent circuitry provides the substrate for generating neuronal activity, whereas interactions with distributed cortical and subcortical networks determine how this activity is integrated, diversified and coordinated at larger scales.

The epilepsy experiments demonstrate that recurrent glutamatergic circuitry participates in the generation of spontaneous population activity in the isolated human cortex. The same-patient in-vivo/in vitro experiments extend this observation by showing that local circuitry also retains the capacity for oscillatory synchronization after removal from the intact brain. Thus, population events and gamma coordination are not necessarily

imported from large-scale networks. At the same time, isolation greatly reduces population coupling, functional connectivity and dimensionality. The intact brain, consequently, contributes something different from simply driving local activity: it expands the repertory of available network states and embeds local circuits within a larger communication architecture. This provides a useful conceptual distinction between generation and organization. Local circuits generate coordinated activity, while distributed networks determine how independently generated local dynamics interact, diversify and contribute to global cortical computation (151).

The observation that neuronal density predicts population coupling in vivo but not after isolation further supports this hierarchical interpretation. Anatomical organization provides the substrate for functional interactions, but its functional expression relies on ongoing communication with the broader network. Likewise, preserved laminar gamma generators indicate that local architecture contains the machinery for oscillation generation, while the increased gamma synchronization observed after isolation suggests that large-scale inputs normally constrain or diversify this intrinsic tendency.

The epilepsy findings fit within the same framework. Epileptic tissue retains the intrinsic capacity for coordinated activity but exhibits altered dependence on glutamatergic mechanisms and changes in neuronal firing organization. Pathology can therefore be viewed not simply as the creation of an abnormal activity mechanism, but as a modification of the activity of an intrinsic cortical network.

Overall, the findings support a hierarchical model in which molecular and cellular properties establish the substrate of local circuitry, and recurrent excitation and inhibition generate neuronal ensembles and oscillations but distributed cortical and thalamocortical interactions are critically needed to integrate these local dynamics into higher-dimensional population activity. The cortex is therefore neither purely a collection of autonomous microcircuits nor simply a passive component of a large-scale network. Its dynamics emerge from continuous interaction between these organizational levels.

5.4 Strengths and limitations

A major strength of the thesis is the combination of complementary experimental scales, as extracellular single unit recordings, LFP and CSD analyses, functional and graph-based network measures, and quantitative histology were integrated within the same experimental framework. The comparison of matched recordings from the same cortical

regions of the same patients during wakefulness, NREM sleep and acute in vitro slices are of particular importance. The same neuronal clusters identified within different in vivo states further provide a strong basis for the investigation of the reduced external input occurring during NREM sleep.

The combination of electrophysiology and histology also allowed functional measures to be related to cortical lamination and cellular organization. The use of standardized analysis workflows and the development of a graphical interface for electrophysiological analysis further support reproducibility and systematic processing of human extracellular recordings. The methodological framework developed in **Article I** and the accompanying methodological work provide a practical foundation for spike sorting and downstream single-unit analysis.

Several limitations should nevertheless be considered. Human tissue is necessarily heterogeneous with respect to age, pathology, medication history, cortical region and surgical context (125). Sample sizes were also limited, particularly for pharmacological experiments, monosynaptic connectivity and histological correlations. Consequently, negative results should not be interpreted as definitive evidence for the absence of an effect.

Acute slice preparation introduces additional biological perturbations beyond the intended removal of long-range inputs, including axotomy, altered extracellular environment and partial disruption of local connectivity (12, 79). The present experiments therefore cannot identify which changes are caused specifically by loss of long-range input and which reflect the slice preparation or maintenance itself. The histological preservation of neuronal density provides evidence against extensive cell loss, but does not exclude functional or synaptic alterations induced by tissue isolation.

Similarly, extracellular cell type classification remains probabilistic, and putative connectivity inferred from cross-correlograms cannot substitute for direct anatomical confirmation. The graph measures should therefore be interpreted as descriptions of functional organization rather than direct reconstructions of anatomical connectivity.

Finally, the mesoscopic model intentionally reduces cortical dynamics to a small number of interpretable parameters. Its value lies in demonstrating that the observed dissociation between population coupling and gamma synchronization can emerge from separable

mechanisms and not providing a complete mechanistic reconstruction of the human cortex. The model should therefore be regarded as a hypothesis-generating framework.

5.5 Translational and methodological implications

Beyond the basic biological conclusions, the findings have implications for both human electrophysiology and translational neuroscience. Acute human cortical slices provide direct access to intrinsic human microcircuits, representing valuable preparation for studying cellular and network mechanisms that cannot readily be isolated in vivo. At the same time, the present results demonstrate that slice activity should not be interpreted as a direct surrogate for intact cortical dynamics. The strong increase in gamma synchronization and simultaneous reduction in population coupling illustrate that isolated tissue may preserve local mechanisms while occupying a substantially different network regulation. As such, this distinction is particularly relevant for epilepsy research. Pharmacological manipulation of human tissue can reveal disease-associated changes in receptor dependence and recurrent excitation that are difficult to infer from in vivo recordings alone (152). Conversely, the intact-brain recordings demonstrate which features of neuronal organization depend on distributed network embedding. Combining both approaches may therefore provide a more informative framework for identifying pathological mechanisms and evaluating interventions aimed at restoring physiological network organization.

The methodological contributions of the thesis are complementary to these biological findings. Standardized spike-sorting and electrophysiological analysis workflows, together with graphical analysis tools, enable reproducible examination of increasingly large human extracellular datasets: such approaches may become valuable as high-density probes and multimodal recordings make simultaneous cellular and network-level measurements increasingly common.

Ultimately, the translational relevance of these findings lies less in identifying a single pathological mechanism, but in defining the level at which different cortical anomalies emerge. Alterations in receptor function, local connectivity, population integration and large-scale network organization need not produce identical electrophysiological signatures. Distinguishing these levels may improve interpretation of human recordings and help connect cellular mechanisms with clinically observable network dysfunction.

6. CONCLUSIONS

This thesis investigated the structural and functional organization of human neocortical microcircuits by integrating extracellular electrophysiology, quantitative network analysis, and histological characterization across complementary *in vivo* and *in vitro* experimental settings. The development of a consistent spike-sorting workflow and an easily accessible graphical user interface for spike-sorting curation provided a robust methodological framework for the reliable extraction and analysis of single-neuron activity from human extracellular recordings.

The first objective examined how epilepsy alters excitatory neurotransmission in human cortical microcircuits. Pharmacological experiments demonstrated that spontaneous population activity depends critically on recurrent glutamatergic signaling, with NMDA receptor-mediated transmission contributing more prominently to epileptic than non-epileptic cortex. Histological analyses revealed no significant difference in the density of SMI-32-positive pyramidal neurons, suggesting that epilepsy-related functional reorganization can occur without major loss of this excitatory neuronal population.

The second objective investigated respective contributions of intrinsic local circuitry and large-scale brain networks to human cortical dynamics, by comparing recordings obtained in vivo and in vitro from the same cortical regions following surgical resection. Neuronal firing properties, spontaneous population activity, and laminar gamma-band generators were largely preserved in vitro, pointing towards recurrent cortical microcircuits being able to generate coordinated activity. In contrast, functional connectivity, population coupling, and network dimensionality were markedly reduced despite increased local synchronization, highlighting the critical contribution of long-range cortical and subcortical interactions, as well as intact dendritic and axonal arborization to the integrated dynamics of the brain.

Taken together, these findings demonstrate that human cortical function emerges from the interaction between intrinsically active local microcircuits and distributed brain-wide networks. Apart from the experimental considerations, this thesis establishes an integrated methodological framework for investigating human cortical microcircuits and provides a foundation for future studies combining extracellular electrophysiology, quantitative network analysis, and multimodal anatomical characterization in physiological and altered neurological conditions.

7. SUMMARY

The neocortex gives rise to higher cognitive functions through the meticulous orchestration of neuronal microcircuits. Although animal models established the basis of cortical organization, direct exploration of human cortical physiology is hampered by restricted access to human brain tissue. This work attempted to investigate the structural and functional motifs of human neocortical microcircuits by employing extracellular electrophysiology, quantitative network analysis, and histological characterization across complementary *in vivo* and *in vitro* experimental settings.

A prerequisite for all subsequent analyses was the reliable identification of single neurons from extracellular recordings. Accordingly, this work contributed in supporting spike-sorting and post-processing through a comprehensive methodological review and the development of an easily accessible graphical user interface for spike-sorting curation, providing a robust analytical framework for further experimental studies.

The first experimental objective examined how epilepsy alters excitatory neurotransmission in the human neocortex. Pharmacological experiments demonstrated that spontaneous population activity significantly depends on recurrent glutamatergic signaling and that NMDA receptor-mediated transmission contributes more prominently in epileptic than in non-epileptic cortex. Preserved density of histologically identified pyramidal cells further supported a sustained cellular architecture of excitatory cortical microcircuits.

The second objective explored how intrinsic local circuitry and large-scale brain networks shape human cortical dynamics by comparing recordings taken *in vivo* with those from the same cortical regions, following surgical removal. While neuronal firing, spontaneous population activity, and laminar gamma-band generators were largely preserved *in vitro*, functional connectivity, population coupling, and network dimensionality were markedly reduced despite increased local synchronization.

All in all, these findings support that recurrent cortical microcircuits do intrinsically generate coordinated neuronal activity, but at the same time, long-range brain-wide interactions are essential for the functional integration and complexity owned by the intact human cortex. Beyond these biological insights, this work offers methodological improvements and an integrated framework for studying human cortical microcircuits in health and neurological disease.

8. REFERENCES

1. Douglas RJ, Martin KAC. Neuronal Circuits of the Neocortex. Annu Rev Neurosci. 2004; 27(1):419–51.
2. Harris KD, Shepherd GMG. The neocortical circuit: themes and variations. Nat Neurosci. 2015; 18(2):170–81.
3. Qian X, Coleman K, Jiang S, Kriz AJ, Marciano JH, Luo C, et al. Spatial transcriptomics reveals human cortical layer and area specification. Nature. 2025; 644(8075):153–63.
4. Tore M, Monni L, Clemente A Di, Giugliano M. Enhanced information processing in the human neocortex: cellular mechanisms and translational perspectives. Frontiers in Synaptic Neuroscience. Frontiers Media SA; 2026.
5. Sherman SM. Thalamus plays a central role in ongoing cortical functioning. Nat Neurosci. 2016; 19(4):533–41.
6. Hwang K, Bertolero MA, Liu WB, D'Esposito M. The Human Thalamus Is an Integrative Hub for Functional Brain Networks. The Journal of Neuroscience. 2017; 37(23):5594–607.
7. Kalmbach BE, Buchin A, Long B, Close J, Nandi A, Miller JA, et al. h-Channels Contribute to Divergent Intrinsic Membrane Properties of Supragranular Pyramidal Neurons in Human versus Mouse Cerebral Cortex. Neuron. Cell Press; 2018; 100(5):1194-1208.e5.
8. Eichler A, Kruse P, Schob C, Lenz M. Synaptic transmission in supragranular layers of the human cortex – comparative review of structure, function, and plasticity. Frontiers in Synaptic Neuroscience. Frontiers Media SA; 2025.
9. Szegedi V, Paizs M, Baka J, Barzó P, Molnár G, Tamas G, et al. Robust perisomatic GABAergic selfinnervation inhibits basket cells in the human and mouse supragranular neocortex. Elife. eLife Sciences Publications Ltd; 2020; 9.
10. Spruston N. Pyramidal neurons: Dendritic structure and synaptic integration. Nature Reviews Neuroscience. 2008.
11. Chen JY, Chauvette S, Skorheim S, Timofeev I, Bazhenov M. Interneuron-mediated inhibition synchronizes neuronal activity during slow oscillation. Journal of Physiology. 2012; 590(16):3987–4010.

12. la Prida LM de, Huberfeld G. Inhibition and oscillations in the human brain tissue in vitro. Neurobiol Dis. 2019; 125:198–210.
13. Defelipe J, López-Cruz PL, Benavides-Piccione R, Bielza C, Larrañaga P, Anderson S, et al. New insights into the classification and nomenclature of cortical GABAergic interneurons. Nat Rev Neurosci. 2013; 14(3):202–16.
14. Bartos M, Vida I, Jonas P. Synaptic mechanisms of synchronized gamma oscillations in inhibitory interneuron networks. Nature Reviews Neuroscience. 2007.
15. Rudy B, Fishell G, Lee S, Hjerling-Leffler J. Three groups of interneurons account for nearly 100% of neocortical GABAergic neurons. Dev Neurobiol. 2011; 71(1):45–61.
16. Cardin JA. Inhibitory Interneurons Regulate Temporal Precision and Correlations in Cortical Circuits. Trends Neurosci. 2018; 41(10):689–700.
17. Tasic B, Yao Z, Graybuck LT, Smith KA, Nguyen TN, Bertagnolli D, et al. Shared and distinct transcriptomic cell types across neocortical areas. Nature. Nature Publishing Group; 2018; 563(7729):72–8.
18. Bugeon S, Duffield J, Dipoppa M, Ritoux A, Prankerd I, Nicoloutsopoulos D, et al. A transcriptomic axis predicts state modulation of cortical interneurons. Nature. Nature Research; 2022; 607(7918):330–8.
19. Harris KD, Mrsic-Flogel TD. Cortical connectivity and sensory coding. Nature. 2013; 503(7474):51–8.
20. Wang Y, Wang Q, Zheng R, Xu X, Yang X, Gui Q, et al. Flexible multichannel electrodes for acute recording in nonhuman primates. Microsyst Nanoeng. Springer Nature; 2023; 9(1).
21. Mohan H, Verhoog MB, Doreswamy KK, Eyal G, Aardse R, Lodder BN, et al. Dendritic and Axonal Architecture of Individual Pyramidal Neurons across Layers of Adult Human Neocortex. Cerebral Cortex. 2015; 25(12):4839–53.
22. Beaulieu-Laroche L, Toloza EHS, Goes MS van der, Lafourcade M, Barnagian D, Williams ZM, et al. Enhanced Dendritic Compartmentalization in Human Cortical Neurons. Cell. Cell Press; 2018; 175(3):643-651.e14.

23. Gidon A, Zolnik TA, Fidzinski P, Bolduan F, Papoutsi A, Poirazi P, et al. Dendritic action potentials and computation in human layer 2/3 cortical neurons. Science (1979). 2020; 367(6473):83–7.
24. Eyal G, Verhoog MB, Testa-Silva G, Deitcher Y, Lodder JC, Benavides-Piccione R, et al. Unique membrane properties and enhanced signal processing in human neocortical neurons. Elife. 2016; 5.
25. Peng Y, Bjelde A, Aceituno PV, Mittermaier FX, Planert H, Grosser S, et al. Directed and acyclic synaptic connectivity in the human layer 2-3 cortical microcircuit. Science (1979). 2024; 384(6693):338–43.
26. Zhang Y, Yu H, Windolf C, Whiteway MR, Wang S, Varol E, et al. A brain-wide map of neural activity during complex behaviour. Nature. Nature Research; 2025; 645(8079):177–91.
27. Buzsáki G. Rhythms of the Brain. Oxford University Press; 2006.
28. Thut G, Miniussi C, Gross J. The Functional Importance of Rhythmic Activity in the Brain. Current Biology. 2012; 22(16):R658–63.
29. Buzsáki G, Draguhn A. Neuronal oscillations in cortical networks. Science. 2004; 304(5679):1926–9.
30. Neves L, Lobão-Soares B, Araujo AP de C, Furtunato AMB, Paiva I, Souza N, et al. Theta and gamma oscillations in the rat hippocampus support the discrimination of object displacement in a recognition memory task. Front Behav Neurosci. Frontiers Media S.A.; 2022; 16.
31. Csercsa R, Dombovári B, Fabó D, Wittner L, Erss L, Entz L, et al. Laminar analysis of slow wave activity in humans. Brain. Oxford University Press; 2010; 133(9):2814–29.
32. Buzsáki G, Moser EI. Memory, navigation and theta rhythm in the hippocampal-entorhinal system. Nat Neurosci. 2013; 16(2):130–8.
33. Fernandez-Ruiz A, Sirota A, Lopes-dos-Santos V, Dupret D. Over and above frequency: Gamma oscillations as units of neural circuit operations. Neuron. Cell Press; 2023.
34. Sohal VS, Zhang F, Yizhar O, Deisseroth K. Parvalbumin neurons and gamma rhythms enhance cortical circuit performance. Nature. 2009; 459(7247):698–702.

35. Traub RD, Jefferys JGR, Whittington MA. Simulation of Gamma Rhythms in Networks of Interneurons and Pyramidal Cells. Journal of Computational Neuroscience. Kluwer Academic Publishers; 1997.
36. Canolty RT, Edwards E, Dalal SS, Soltani M, Nagarajan SS, Kirsch HE, et al. High gamma power is phase-locked to theta oscillations in human neocortex. Science (1979). 2006; 313(5793):1626–8.
37. Hájos N, Pálhalini J, Mann EO, Nèmeth B, Paulsen O, Freund TF. Spike timing of distinct types of GABAergic interneuron during hippocampal gamma oscillations in vitro. Journal of Neuroscience. 2004; 24(41):9127–37.
38. Buzsáki G, Anastassiou CA, Koch C. The origin of extracellular fields and currents-EEG, ECoG, LFP and spikes. Nature Reviews Neuroscience. 2012.
39. Herreras O. Local field potentials: Myths and misunderstandings. Front Neural Circuits. Frontiers Media S.A.; 2016; 10(DEC).
40. Kadir LA, Stacey M, Barrett-Jolley R. Emerging roles of the membrane potential: Action beyond the action potential. Frontiers in Physiology. Frontiers Media S.A.; 2018.
41. Raghavan M, Fee D, Barkhaus PE. Generation and propagation of the action potential. In: Handbook of Clinical Neurology. Elsevier B.V.; 2019; bk. 160, p. 3–22.
42. García-Prieto J, Bajo R, Pereda E. Efficient computation of functional brain networks: Toward real-time functional connectivity. Front Neuroinform. Frontiers Research Foundation; 2017; 11.
43. Galakhova AA, Hunt S, Wilbers R, Heyer DB, Kock CPJ de, Mansvelder HD, et al. Evolution of cortical neurons supporting human cognition. Trends Cogn Sci. 2022; 26(11):909–22.
44. Loomba S, Straehle J, Gangadharan V, Heike N, Khalifa A, Motta A, et al. Connectomic comparison of mouse and human cortex. Science (1979). 2022; 377(6602).
45. Benavides-Piccione R, Blazquez-Llorca L, Kastanauskaite A, Fernaud-Espinosa I, Tapia-González S, DeFelipe J. Key morphological features of human pyramidal neurons. Cerebral Cortex. 2024; 34(5).

46. Aizenbud I, Yoeli D, Beniaguev D, Kock CPJ de, London M, Segev I. Dendritic morphology and synaptic nonlinearities enhance functional complexity in human cortical neurons. Proceedings of the National Academy of Sciences. 2026; 123(28).
47. Boldog E, Bakken TE, Hodge RD, Novotny M, Aevermann BD, Baka J, et al. Transcriptomic and morphophysiological evidence for a specialized human cortical GABAergic cell type. Nat Neurosci. 2018; 21(9):1185–95.
48. Cash SS, Halgren E, Dehghani N, Rossetti AO, Thesen T, Wang C, et al. The Human K-Complex Represents an Isolated Cortical Down-State. Science (1979). 2009; 324(5930):1084–7.
49. Keller CJ, Truccolo W, Gale JT, Eskandar E, Thesen T, Carlson C, et al. Heterogeneous neuronal firing patterns during interictal epileptiform discharges in the human cortex. Brain. 2010; 133(6):1668–81.
50. Pillai J, Sperling MR. Interictal EEG and the diagnosis of epilepsy. Epilepsia. 2006.
51. Moon H, Kwon J, Eun J, Chung CK, Kim JS, Chou N, et al. Electrocorticogram (ECoG): Engineering Approaches and Clinical Challenges for Translational Medicine. Adv Mater Technol. 2024; 9(12).
52. Kim GH, Kim K, Lee E, An T, Choi WS, Lim G, et al. Recent progress on microelectrodes in neural interfaces. Materials. MDPI AG; 2018.
53. Wang Y, Yang X, Zhang X, Wang Y, Pei W. Implantable intracortical microelectrodes: reviewing the present with a focus on the future. Microsystems and Nanoengineering. Springer Nature; 2023.
54. Fabo D, Bokodi V, Szabó JP, Tóth E, Salami P, Keller CJ, et al. The role of superficial and deep layers in the generation of high frequency oscillations and interictal epileptiform discharges in the human cortex. Sci Rep. Nature Research; 2023; 13(1).
55. Ulbert I, Halgren E, Heit G, Karmos G. Multiple microelectrode-recording system for human intracortical applications. J Neurosci Methods. 2001; 106(1):69–79.
56. Es MWJ van, Higgins C, Gohil C, Quinn AJ, Vidaurre D, Woolrich MW. Large-scale cortical functional networks are organized in structured cycles. Nat Neurosci. Nature Research; 2025; 28(10):2118–28.

57. Verzi SJ, Rothganger F, Parekh OD, Quach TT, Miner NE, Vineyard CM, et al. Computing with spikes: The advantage of fine-grained timing. Neural Computation. MIT Press Journals; 2018.
58. Rey HG, Pedreira C, Quian Quiroga R. Past, present and future of spike sorting techniques. Brain Research Bulletin. Elsevier Inc.; 2015.
59. Quiroga RQ, Nadasdy Z, Ben-Shaul Y. Unsupervised Spike Detection and Sorting with Wavelets and Superparamagnetic Clustering. Neural Comput. 2004; 16(8):1661–87.
60. Barthó P, Hirase H, Monconduit L, Zugaro M, Harris KD, Buzsáki G. Characterization of neocortical principal cells and interneurons by network interactions and extracellular features. J Neurophysiol. 2004; 92(1):600–8.
61. Steinmetz NA, Aydin C, Lebedeva A, Okun M, Pachitariu M, Bauza M, et al. Neuropixels 2.0: A miniaturized high-density probe for stable, long-term brain recordings. Science (1979). American Association for the Advancement of Science; 2021; 372(6539).
62. Meisel C, Olbrich E, Shriki O, Achermann P. Fading signatures of critical brain dynamics during sustained wakefulness in humans. Journal of Neuroscience. 2013; 33(44):17363–72.
63. Poulet JFA, Crochet S. The cortical states of wakefulness. Frontiers in Systems Neuroscience. Frontiers Media S.A.; 2019.
64. Sacha M, Goldman JS, Kusch L, Destexhe A. Asynchronous and Slow-Wave Oscillatory States in Connectome-Based Models of Mouse, Monkey and Human Cerebral Cortex. Applied Sciences (Switzerland). Multidisciplinary Digital Publishing Institute (MDPI); 2024; 14(3).
65. Chiong W, Leonard MK, Chang EF. Neurosurgical Patients as Human Research Subjects: Ethical Considerations in Intracranial Electrophysiology Research. Neurosurgery. 2018; 83(1):29–37.
66. Fox KCR, Foster BL, Kucyi A, Daitch AL, Parvizi J. Intracranial Electrophysiology of the Human Default Network. Trends Cogn Sci. 2018; 22(4):307–24.

67. Okun M, Steinmetz NA, Cossell L, Iacaruso MF, Ko H, Barthó P, et al. Diverse coupling of neurons to populations in sensory cortex. Nature. Nature Publishing Group; 2015; 521(7553):511–5.
68. O'Connor D, Mandino F, Shen X, Horien C, Ge X, Herman P, et al. Functional network properties derived from wide-field calcium imaging differ with wakefulness and across cell type. Neuroimage. Academic Press Inc.; 2022; 264.
69. György Buzsáki. The Brain from Inside Out. Oxford: Oxford University Press; 2019.
70. Luppi P-H, Fort P. Sleep–wake physiology. In: Handbook of Clinical Neurology. 2019; p. 359–70.
71. Chauvette S, Volgushev M, Timofeev I. Origin of Active States in Local Neocortical Networks during Slow Sleep Oscillation. Cerebral Cortex. 2010; 20(11):2660–74.
72. Steriade M, McCormick DA, Sejnowski TJ. Thalamocortical Oscillations in the Sleeping and Aroused Brain. Science (1979). 1993; 262(5134):679–85.
73. Barttfelda P, Uhriga L, Sitta JD, Sigmane M, Jarrayaa B, Dehaene S. Signature of consciousness in the dynamics of resting-state brain activity. Proc Natl Acad Sci U S A. National Academy of Sciences; 2015; 112(3):887–92.
74. Fontenele AJ, Sooter JS, Norman VK, Gautam SH, Shew WL. Low-dimensional criticality embedded in high-dimensional awake brain dynamics. Sci Adv. 2024; 10(17).
75. Sinton CM, McCarley RW. Neurophysiological Mechanisms of Sleep and Wakefulness: A Question of Balance. Semin Neurol. 2004; 24(3):211–23.
76. Timofeev I. Origin of Slow Cortical Oscillations in Deafferented Cortical Slabs. Cerebral Cortex. 2000; 10(12):1185–99.
77. Wilbers R, Metodieva VD, Duverdin S, Heyer DB, Galakhova AA, Mertens EJ, et al. Human voltage-gated Na^+ and K^+ channel properties underlie sustained fast AP signaling. Sci Adv. 2023; 9(41).
78. Molnár G, Oláh S, Komlósi G, Füle M, Szabadics J, Varga C, et al. Complex Events Initiated by Individual Spikes in the Human Cerebral Cortex. PLoS Biol. 2008; 6(9):e222.

79. Belle AM, Enright HA, Sales AP, Kulp K, Osburn J, Kuhn EA, et al. Evaluation of in vitro neuronal platforms as surrogates for in vivo whole brain systems. Sci Rep. Nature Publishing Group; 2018; 8(1).
80. Köhling R, Avoli M. Methodological approaches to exploring epileptic disorders in the human brain in vitro. Journal of Neuroscience Methods. 2006.
81. Howard D, Chameh HM, Guet-Mccreight A, Hsiao HA, Vuong M, Seo YS, et al. An in vitro whole-cell electrophysiology dataset of human cortical neurons. Gigascience. Oxford University Press; 2022; 11.
82. Kodandaramaiah SB, Holst GL, Wickersham IR, Singer AC, Franzesi GT, McKinnon ML, et al. Assembly and operation of the autopatcher for automated intracellular neural recording in vivo. Nat Protoc. Nature Publishing Group; 2016; 11(4):634–54.
83. Kapucu FE, Mäkinen MEL, Tanskanen JMA, Ylä-Outinen L, Narkilahti S, Hyttinen JAK. Joint analysis of extracellular spike waveforms and neuronal network bursts. J Neurosci Methods. Elsevier; 2016; 259:143–55.
84. Henze DA, Borhegyi Z, Csicsvari J, Mamiya A, Harris KD, Buzsáki G. Intracellular features predicted by extracellular recordings in the hippocampus in vivo. J Neurophysiol. 2000; 84(1):390–400.
85. Despouy E, Curot J, Reddy L, Nowak LG, Deudon M, Sol JC, et al. Recording local field potential and neuronal activity with tetrodes in epileptic patients. J Neurosci Methods. Elsevier B.V.; 2020; 341.
86. Fiáth R, Raducanu BC, Musa S, Andrei A, Lopez CM, Hoof C van, et al. A silicon-based neural probe with densely-packed low-impedance titanium nitride microelectrodes for ultrahigh-resolution in vivo recordings. Biosens Bioelectron. Elsevier Ltd; 2018; 106:86–92.
87. Okun M, Lak A, Carandini M, Harris KD. Long term recordings with immobile silicon probes in the mouse cortex. PLoS One. Public Library of Science; 2016; 11(3).
88. Neto JP, Lopes G, Frazão J, Nogueira J, Lacerda P, Baião P, et al. Validating silicon polytrodes with paired juxtacellular recordings: method and dataset. J Neurophysiol. 2016; 116(2):892–903.

89. Bod RB, Rokai J, Meszéna D, Fiáth R, Ulbert I, Márton G. From End to End: Gaining, Sorting, and Employing High-Density Neural Single Unit Recordings. Frontiers in Neuroinformatics. Frontiers Media S.A.; 2022.
90. Gibson S, Judy JW, Marković D. Spike sorting: The first step in decoding the brain: The first step in decoding the brain. IEEE Signal Process Mag. Institute of Electrical and Electronics Engineers Inc.; 2012; 29(1):124–43.
91. Rossant C, Kadir SN, Goodman DFM, Schulman J, Hunter MLD, Saleem AB, et al. Spike sorting for large, dense electrode arrays. Nat Neurosci. 2016; 19(4):634–41.
92. Pachitariu M, Sridhar S, Pennington J, Stringer C. Spike sorting with Kilosort4. Nat Methods. 2024; 21(5):914–21.
93. Saif-Ur-Rehman M, Ali O, Dyck S, Lienkämper R, Metzler M, Parpaley Y, et al. SpikeDeep-classifier: A deep-learning based fully automatic offline spike sorting algorithm. J Neural Eng. IOP Publishing Ltd; 2021; 18(1).
94. Rokai J, Rácz M, Fiáth R, Ulbert I, Márton G. Elvisort: Encoding latent variables for instant sorting, an artificial intelligence-based end-to-end solution. J Neural Eng. IOP Publishing Ltd; 2021; 18(4).
95. Rácz M, Liber C, Németh E, Fiáth R, Rokai J, Harmati I, et al. Spike detection and sorting with deep learning. Journal of Neural Engineering. Institute of Physics Publishing; 2020.
96. Lee J, Mitelut C, Shokri H, Kinsella I, Dethe N, Wu S, et al. YASS: Yet Another Spike Sorter applied to large-scale multi-electrode array recordings in primate retina [Internet]. 2020. Available from: http://biorxiv.org/lookup/doi/10.1101/2020.03.18.997924.
97. Windolf C, Yu H, Paulk AC, Meszéna D, Muñoz W, Boussard J, et al. DREDge: robust motion correction for high-density extracellular recordings across species. Nat Methods. 2025; 22(4):788–800.
98. Barnett AH, Magland JF, Greengard LF. Validation of neural spike sorting algorithms without ground-truth information. J Neurosci Methods. Elsevier B.V.; 2016; 264:65–77.

99. Buccino AP, Hurwitz CL, Garcia S, Magland J, Siegle JH, Hurwitz R, et al. Spikeinterface, a unified framework for spike sorting. Elife. eLife Sciences Publications Ltd; 2020; 9:1–24.
100. Magland J, Jun JJ, Lovero E, Morley AJ, Hurwitz CL, Buccino AP, et al. Spikeforest, reproducible web-facing ground-truth validation of automated neural spike sorters. Elife. eLife Sciences Publications Ltd; 2020; 9.
101. Baroni F, Fulcher BD. Synchrony, oscillations, and phase relationships in collective neuronal activity: A highly comparative overview of methods. PLoS Comput Biol. 2025; 21(10):e1013597.
102. Das A, Zabeh E, Jacobs J. How to Detect and Analyze Traveling Waves in Human Intracranial EEG Oscillations? 2023; p. 487–505.
103. Fries P, Reynolds JH, Rorie AE, Desimone R. Modulation of Oscillatory Neuronal Synchronization by Selective Visual Attention. Science (1979). 2001; 291(5508):1560–3.
104. Safavi S, Panagiotaropoulos TI, Kapoor V, Ramirez-Villegas JF, Logothetis NK, Besserve M. Uncovering the organization of neural circuits with Generalized Phase Locking Analysis. PLoS Comput Biol. Public Library of Science; 2023; 19(4).
105. McGinn RJ, Valiante TA. Phase-amplitude coupling and interlaminar synchrony are correlated in human neocortex. Journal of Neuroscience. Society for Neuroscience; 2014; 34(48):15923–30.
106. Womelsdorf T, Schoffelen J-M, Oostenveld R, Singer W, Desimone R, Engel AK, et al. Modulation of Neuronal Interactions Through Neuronal Synchronization. Science (1979). 2007; 316(5831):1609–12.
107. Huh CYL, Amilhon B, Ferguson KA, Manseau F, Torres-Platas SG, Peach JP, et al. Excitatory Inputs Determine Phase-Locking Strength and Spike-Timing of CA1 Stratum Oriens/Alveus Parvalbumin and Somatostatin Interneurons during Intrinsically Generated Hippocampal Theta Rhythm. The Journal of Neuroscience. 2016; 36(25):6605–22.
108. Guzman E, Cheng Z, Hansma PK, Tovar KR, Petzold LR, Kosik KS. Extracellular detection of neuronal coupling. Sci Rep. Nature Research; 2021; 11(1).

109. Feldt S, Bonifazi P, Cossart R. Dissecting functional connectivity of neuronal microcircuits: experimental and theoretical insights. Trends Neurosci. 2011; 34(5):225–36.
110. Bastos AM, Schoffelen J-M. A Tutorial Review of Functional Connectivity Analysis Methods and Their Interpretational Pitfalls. Front Syst Neurosci. 2016; 9.
111. Cunningham JP, Yu BM. Dimensionality reduction for large-scale neural recordings. Nat Neurosci. 2014; 17(11):1500–9.
112. Gallego JA, Perich MG, Miller LE, Solla SA. Neural Manifolds for the Control of Movement. Neuron. 2017; 94(5):978–84.
113. Tóth K, Hofer KT, Kandrács Á, Entz L, Bagó A, Erőss L, et al. Hyperexcitability of the network contributes to synchronization processes in the human epileptic neocortex. Journal of Physiology. Blackwell Publishing Ltd; 2018; 596(2):317–42.
114. Cardin JA. Inhibitory Interneurons Regulate Temporal Precision and Correlations in Cortical Circuits. Trends Neurosci. 2018; 41(10):689–700.
115. Rudy B, Fishell G, Lee S, Hjerling-Leffler J. Three groups of interneurons account for nearly 100% of neocortical GABAergic neurons. Dev Neurobiol. 2011; 71(1):45–61.
116. Mühlebner A, Iyer AM, Scheppingen J van, Anink JJ, Jansen FE, Veersema TJ, et al. Specific pattern of maturation and differentiation in the formation of cortical tubers in tuberous sclerosis complex (TSC): evidence from layer-specific marker expression. J Neurodev Disord. 2016; 8(1):9.
117. Campbell MJ, Morrison JH. Monoclonal antibody to neurofilament protein (SMI-32) labels a subpopulation of pyramidal neurons in the human and monkey neocortex. Journal of Comparative Neurology. 1989; 282(2):191–205.
118. Toth M, Papp KS, Gede N, Farkas K, Kovacs S, Isnard J, et al. Surgical outcomes related to invasive EEG monitoring with subdural grids or depth electrodes in adults: A systematic review and meta-analysis. Seizure. W.B. Saunders Ltd; 2019; 70:12–9.
119. Engel AK, Moll CKE, Fried I, Ojemann GA. Invasive recordings from the human brain: clinical insights and beyond. Nat Rev Neurosci. 2005; 6(1):35–47.
120. Chari A, Thornton RC, Tisdall MM, Scott RC. Microelectrode recordings in human epilepsy: a case for clinical translation. Brain Commun. 2020; 2(2).

121. Dwivedi AK, Mahesh A, Sanfeliu A, Larkin J, Siwicki RA, Sweeney KJ, et al. High-resolution multimodal profiling of human epileptic brain activity via explanted depth electrodes. JCI Insight. 2025; 10(1).
122. Jones RSG, Silva AB da, Whittaker RG, Woodhall GL, Cunningham MO. Human brain slices for epilepsy research: Pitfalls, solutions and future challenges. Journal of Neuroscience Methods. Elsevier; 2016.
123. Wickham J, Brödjegård NG, Vighagen R, Pinborg LH, Bengzon J, Woldbye DPD, et al. Prolonged life of human acute hippocampal slices from temporal lobe epilepsy surgery. Sci Rep. 2018; 8(1):4158.
124. Hart MG, Romero-Garcia R, Price SJ, Suckling J. Global Effects of Focal Brain Tumors on Functional Complexity and Network Robustness: A Prospective Cohort Study. Neurosurgery. 2019; 84(6):1201–13.
125. Avoli M, Williamson A. Functional and pharmacological properties of human neocortical neurons maintained in vitro. Prog Neurobiol. 1996; 48(6):519–54.
126. Ting JT, Kalmbach B, Chong P, Frates R de, Keene CD, Gwinn RP, et al. A robust ex vivo experimental platform for molecular-genetic dissection of adult human neocortical cell types and circuits. Sci Rep. 2018; 8(1):8407.
127. Yang D, Feldmeyer D. Rhythmic network activity in human brain slices: variability, mechanisms, and translational insights. Frontiers in Synaptic Neuroscience. Frontiers Media SA; 2026.
128. Bod R, Tóth K, Essam N, Tóth EZ, Erõss L, Entz L, et al. Synaptic alterations and neuronal firing in human epileptic neocortical excitatory networks. Front Synaptic Neurosci. Frontiers Media SA; 2023; 15.
129. Kandrács Á, Hofer KT, Tóth K, Tóth EZ, Entz L, Bagó AG, et al. Presence of synchrony-generating hubs in the human epileptic neocortex. Journal of Physiology. Blackwell Publishing Ltd; 2019; 597(23):5639–70.
130. Hofer KT, Kandrács Á, Tóth K, Hajnal B, Bokodi V, Tóth EZ, et al. Bursting of excitatory cells is linked to interictal epileptic discharge generation in humans. Sci Rep. Nature Research; 2022; 12(1).
131. Wittner L, Huberfeld G, Clémenceau S, Erőss L, Dezamis E, Entz L, et al. The epileptic human hippocampal cornu ammonis 2 region generates spontaneous interictal-like activity in vitro. Brain. 2009; 132(11):3032–46.

132. Buccino AP, Hurwitz CL, Garcia S, Magland J, Siegle JH, Hurwitz R, et al. Spikeinterface, a unified framework for spike sorting. Elife. eLife Sciences Publications Ltd; 2020; 9:1–24.
133. Tóth K, Hofer KT, Kandrács Á, Entz L, Bagó A, Erőss L, et al. Hyperexcitability of the network contributes to synchronization processes in the human epileptic neocortex. Journal of Physiology. Blackwell Publishing Ltd; 2018; 596(2):317–42.
134. Thom M, Martinian L, Sen A, Cross JH, Harding BN, Sisodiya SM. Cortical neuronal densities and lamination in focal cortical dysplasia. Acta Neuropathol. 2005; 110(4):383–92.
135. Molnár G, Oláh S, Komlósi G, Füle M, Szabadics J, Varga C, et al. Complex Events Initiated by Individual Spikes in the Human Cerebral Cortex. PLoS Biol. 2008; 6(9):e222.
136. Sanchez-Vives M V., McCormick DA. Cellular and network mechanisms of rhythmic recurrent activity in neocortex. Nat Neurosci. 2000; 3(10):1027–34.
137. Kalitzin S, Petkov G, Suffczynski P, Grigorovsky V, Bardakjian BL, Lopes da Silva F, et al. Epilepsy as a manifestation of a multistate network of oscillatory systems. Neurobiol Dis. 2019; 130:104488.
138. Guo X, Yu H, Kodama NX, Wang J, Galán RF. Fluctuation Scaling of Neuronal Firing and Bursting in Spontaneously Active Brain Circuits. Int J Neural Syst. World Scientific Publishing Co. Pte Ltd; 2020; 30(1).
139. Schevon CA, Ng SK, Cappell J, Goodman RR, Mckhann G, Waziri A, et al. Microphysiology of Epileptiform Activity in Human Neocortex. J Clin Neurophysiol. 2008.
140. Scheibel ME, Crandall PH, Scheibel AB. The Hippocampal-Dentate Complex in Temporal Lobe Epilepsy. Epilepsia. 1974; 15(1):55–80.
141. Siddiqui AH, Joseph SA. CA3 axonal sprouting in kainate-induced chronic epilepsy. Brain Res. 2005; 1066(1–2):129–46.
142. Perez Y, Morin F, Beaulieu C, Lacaille J. Axonal Sprouting of CA1 Pyramidal Cells in Hyperexcitable Hippocampal Slices of Kainate-treated Rats. European Journal of Neuroscience. 1996; 8(4):736–48.

143. Merricks EM, Smith EH, Emerson RG, Bateman LM, McKhann GM, Goodman RR, et al. Neuronal firing and waveform alterations through Ictal recruitment in humans. Journal of Neuroscience. Society for Neuroscience; 2021; 41(4):766–79.
144. Buzsáki G, Wang XJ. Mechanisms of gamma oscillations. Annual Review of Neuroscience. 2012.
145. Tononi G. Reentry and the problem of cortical integration. Int Rev Neurobiol. 1994; 37:127–52; discussion 203-7.
146. Sporns O. Structure and function of complex brain networks. Dialogues Clin Neurosci. 2013; 15(3):247–62.
147. Stringer C, Pachitariu M, Steinmetz N, Carandini M, Harris KD. High-dimensional geometry of population responses in visual cortex. Nature. Nature Publishing Group; 2019; 571(7765):361–5.
148. Bugeon S, Duffield J, Dipoppa M, Ritoux A, Prankerd I, Nicoloutsopoulos D, et al. A transcriptomic axis predicts state modulation of cortical interneurons. Nature. Nature Research; 2022; 607(7918):330–8.
149. Dahmen D, Layer M, Deutz L, Dąbrowska PA, Voges N, Papen M Von, et al. Global organization of neuronal activity only requires unstructured local connectivity. Elife. eLife Sciences Publications Ltd; 2022; 11.
150. Campagnola L, Seeman SC, Chartrand T, Kim L, Hoggarth A, Gamlin C, et al. Local connectivity and synaptic dynamics in mouse and human neocortex. Science (1979). American Association for the Advancement of Science; 2022; 375(6585).
151. Sederberg A, Pala A, Stanley GB. Latent dynamics of primary sensory cortical population activity structured by fluctuations in the local field potential. Front Comput Neurosci. 2024; 18:1445621.
152. Kiss RJ, Csudor A, Sarosi M, Nagy ZA, Szentes A, Gall Z, et al. Effect of carbamazepine-beta-cyclodextrin inclusion complex on seizure-like events in an in vitro model of temporal lobe epilepsy. Acta Marisiensis - Seria Medica. Sciendo; 2024; 70(2):50–7.

BIBLIOGRAPHY OF THE CANDIDATE'S PUBLICATIONS

Publications related to the thesis:

1. Bod RB, Rokai J, Meszéna D, Fiáth R, Ulbert I, Márton G. From End to End: Gaining, Sorting, and Employing High-Density Neural Single Unit Recordings. Frontiers in Neuroinformatics. Frontiers Media S.A.; 2022.
2. Bod R, Tóth K, Essam N, Tóth EZ, Erőss L, Entz L, et al. Synaptic alterations and neuronal firing in human epileptic neocortical excitatory networks. Front Synaptic Neurosci. Frontiers Media SA; 2023; 15.
3. Bod R, Toth K, Farkas O, Michaeli Y, Toth KZ, Kandracs A, et al. Cortical isolation separates rhythmic synchrony from network integration in the human neocortex. 2026. bioRxiv, doi: https://doi.org/10.64898/2026.09.02.748777

Publications not related to the thesis:

1. Mihály I, Berki ÁJ, Orbán-Kis K, Gáll Z, Bod RB, Szilágyi T. The effect of amygdala low-frequency stimulation on inter-hippocampal connectivity in the pilocarpine model of epilepsy. Acta Marisiensis - Seria Medica. Sciendo; 2021; 67(1):27–33.
2. Mihály I, Orbán-Kis K, Gáll Z, Berki ÁJ, Bod RB, Szilágyi T. Amygdala low-frequency stimulation reduces pathological phase-amplitude coupling in the pilocarpine model of epilepsy. Brain Sci. MDPI AG; 2020; 10(11):1–18.
3. Mihály I, Molnár T, Berki Á-J, Bod R-B, Orbán-Kis K, Gáll Z, et al. Short-Term Amygdala Low-Frequency Stimulation Does not Influence Hippocampal Interneuron Changes Observed in the Pilocarpine Model of Epilepsy and Technology of Târgu Mures [Internet]. 2021. Available from: https://doi.org/10.3390/cells10030520.
4. Gáll Z, Kelemen K, Tolokán A, Zolcseak I, Sável I, Bod R, et al. Anticonvulsant Action and Long-Term Effects of Chronic Cannabidiol Treatment in the Rat Pentylenetetrazole-Kindling Model of Epilepsy. Biomedicines. MDPI; 2022; 10(8).
5. Mihály I, Bod R-B, Orbán-Kis K, Berki Á-J, Szilágyi T. The Effect of Deep Brain Stimulation on High Frequency Oscillations in a Chronic Epilepsy Model. Bulletin of Medical Sciences. Walter de Gruyter GmbH; 2020; 93(2):63–70.
6. Tóth EZ, Stelcz R, Bod R, Petik Á, Juhász E, Tóth K, et al. Preserved functions with profound morphological reorganization in human organotypic cultures. 2026.

ACKNOWLEDGEMENTS

First and foremost, I would like to express my sincere gratitude to my supervisor, Dr. Lucia Wittner. Throughout my studies, she has been an exceptional mentor, combining scientific excellence with wisdom, patience, kindness, and unwavering support. Even when my ideas became somewhat convoluted, she always encouraged me to explore them while providing thoughtful guidance whenever needed. She has been a true role model, both scientifically and personally, and I feel incredibly fortunate to have learned from her.

I am equally grateful to the head of our laboratory, Prof. Dr. István Ulbert, whose creativity, enthusiasm, and sparkling scientific reflections have made the laboratory an inspiring place to work. Together with Dr. Wittner, they created an environment where curiosity was encouraged, new ideas flourished, and doing science remained genuinely enjoyable. Their enthusiasm and commitment to research is something I hope to carry with me for many years.

My heartfelt thanks go to the entire epilepsy team, with whom I shared not only scientific discussions but also the everyday challenges, tiny (and huge) joys of research. I am especially grateful to Dr. Kinga Tóth, Dr. Estilla Tóth, Dr. Ágnes Kandrács, Rebeka Stelcz, Nour Essam, Eszter Juhász, Katalin Tóth and Dr. Domokos Meszéna for their support, amity and inspiration. I would also like to thank everyone in the laboratory for creating such a welcoming and collaborative atmosphere. A special thanks goes to Dr. János Rokai, who convincingly demonstrated that physicians can - and perhaps should - write code.

I am grateful to Dr. László Grand, my industrial supervisor within the Cooperative Doctoral Programme, whose humbleness, insight, and thoughtful advice have been a constant source of inspiration for the past two years.

I would also like to thank the patients who generously donated surgically resected brain tissue for research, as well as the entire neurosurgery team of the Center of Neurosurgery and Neurointervention, whose outstanding medical expertise, time, and meticulous care made this work possible. Their contribution represents an extraordinary gift to science, and without their commitment, the work presented in this thesis would not have been possible.

My deep dive into neuroscience began a bit earlier, rooting back to my undergraduate years in Marosvásárhely. Looking back, I am convinced that without the marvelous

atmosphere and inspiring laboratory community there, I would have chosen a very different path. I am deeply grateful to Dr. István Mihály, Dr. Krisztina Kelemen, Dr. Rita-Judit Kiss, Prof. Dr. Tibor Szilágyi and Dr. Károly Orbán-Kis for introducing me to scientific research, but also the art of medicine with such passion and dedication.

I also owe my gratitude to my parents, who nurtured my curiosity from an early age and taught me the value of constantly cultivating ideas. Their encouragement laid the foundation for everything that followed and follows, as this thesis, after all, is a milestone in the lifelong journey they helped me to begin.

Finally, I would like to thank my beloved husband. Throughout these years, he has been my greatest source of support. Besides constantly expanding my coding toolkit and making sure I never missed the latest technological advances, he created an encouraging environment that made even the most difficult periods easier to overcome. I could not have asked for a better companion for this chapter and probably the next ones to come.

To everyone who contributed to this work, whether through scientific collaboration, friendship, support, or encouragement, thank you. This work is as much a reflection of the people around me as it is of my own efforts.